

Mapping heat vulnerability in Australian capital cities: A machine learning and multi-source data analysis

Fei Li ^a , Tan Yigitcanlar ^{a,*} , Madhav Nepal ^a, Kien Nguyen ^b , Fatih Dur ^a, Wenda Li ^a

^a City 4.0 Lab, School of Architecture and Built Environment, Queensland University of Technology, 2 George Street, Brisbane, QLD 4000, Australia

^b School of Electrical Engineering and Robotics, Queensland University of Technology, 2 George Street, Brisbane, QLD 4000, Australia



ARTICLE INFO

Keywords:

Heat vulnerability
Machine learning
Remote sensing
Thermal equity
Climate change
Australia

ABSTRACT

Heat vulnerability has emerged as a global concern amidst ongoing urbanisation and climate change. While numerous studies have examined heat vulnerability, a gap remains in the application of machine learning to this field. This study aims to address this gap by evaluating the effectiveness of various machine learning algorithms in assessing heat vulnerability across Australian capital cities using heat-related indicators. The findings reveal that: (a) The Random Forest algorithm outperforms the others, achieving a training R^2 of 0.9179 and a testing R^2 of 0.9089, indicating its superior performance in assessing heat vulnerability in Australian capital cities; (b) The spatial analysis reveals significant regional disparities, with higher vulnerability in densely populated urban areas and lower vulnerability in green, less developed suburban and rural areas, necessitating tailored heat mitigation strategies; (c) Heat vulnerability analysis reveals that Australian Capital Territory (ACT) and Greater Darwin (GDRW) have the lowest proportions of highly vulnerable Statistical Area Level 1 (SA1) units, whereas Greater Hobart (GHBA) and Greater Adelaide (GADL) have the highest ones, a clear indication of significant regional disparities, again pointing to tailored mitigation and adaptation strategies; and (d) The sensitivity analysis reveals that personal health conditions and socio-demographic characteristics, such as personal illness status, age, and education level, play dominant roles in determining heat vulnerability, overshadowing the impact of environmental and infrastructural factors. This research provides a comprehensive understanding of heat vulnerability in Australian capital cities and offers valuable insights for urban planners and policymakers to develop data-driven mitigation and adaptation strategies for enhanced urban sustainability and climate resilience.

1. Introduction and background

The growing concern over heat vulnerability has intensified due to rapid urbanisation and climate change, exacerbating the urban heat island (UHI) effect (Bu et al., 2024; Chuang & Gober, 2015; Forceville et al., 2024; Reid et al., 2009). Cities worldwide face escalating heat-related risks, particularly in Europe, North America, Asia, and Oceania, where heat extremes have led to severe consequences. In Europe, the 2003 and 2022 heatwaves caused tens of thousands of deaths, while North America has faced increasingly severe heat events (Ballester et al., 2023; Macintyre et al., 2018; Mallen et al., 2019; Reid et al., 2009). South and Southeast Asia, including India and Pakistan, have endured deadly heat extremes with significant human and economic losses (Bakhsh et al., 2018; Kitchley, 2024). Oceania, particularly

Australia, has experienced record-breaking heat and bushfires, straining urban centres and vulnerable populations (Adnan, 2022; Wang et al., 2023). Research shows urban populations, especially vulnerable groups like the elderly, children, and low-income residents, are disproportionately affected, exacerbating social equity and public health challenges (Aubrecht & Özceylan, 2013; Cheng et al., 2021). Knowledge-based urban development requires addressing vulnerability challenges of these groups (Sarimin & Yigitcanlar, 2012).

Australian capital cities, characterised by high population densities and significant urban development, are particularly susceptible to heat-related risks (Kamruzzaman et al., 2018; Loughnan et al., 2014; Wang et al., 2023). Between 2001 and 2018, heatwaves in Australia caused about 350 deaths, with the elderly being the most affected (Coates et al., 2022). According to the Department of Human Services (2009), the

* Corresponding author.

E-mail addresses: f34.li@hdr.qut.edu.au (F. Li), tan.yigitcanlar@qut.edu.au (T. Yigitcanlar), madhav.nepal@qut.edu.au (M. Nepal), k.nguyenthanh@qut.edu.au (K. Nguyen), f.dur@qut.edu.au (F. Dur), wenda.li@hdr.qut.edu.au (W. Li).

2009 heatwave in Victoria led to a 62 % increase in all-cause mortality and a 12 % increase in overall emergency department presentations. Furthermore, the economic impact of heatwaves is substantial. For instance, heatwave events impose an annual financial burden of approximately \$87 million on the state of Victoria (Victorian Government Department of Environment, Land, Water & Planning, 2019). This substantial cost, which represents 0.025 % of the state's Gross State Product (GSP), arises from increased healthcare expenditures, lost productivity, and infrastructure damage (Economics, 2018). Addressing heat vulnerability in these urban areas is crucial for enhancing public health, promoting social equity, and improving urban resilience against climate change impacts.

Heat vulnerability assessments have gained significant global attention due to the rising impacts of elevated temperatures, particularly frequent and intense heat events, which threaten human health and increase heat-related morbidity and mortality (Cheng et al., 2021; Degirmenci et al., 2021). Various methodologies have been developed to identify vulnerable populations and areas needing urgent intervention, typically involving three processes: indicator selection, modelling, and validation (Li et al., 2022). Indicator selection, a critical foundation for modelling and validation, is guided by the population vulnerability framework and the risk triangle framework (Crichton, 1999; Parry, 2007). The former emphasises exposure, sensitivity, and adaptive capacity, while the latter focuses on hazard, exposure, and vulnerability. Selected indicators often include demographic and socioeconomic factors (e.g., age, income, social isolation, population density) and health-related factors (e.g., chronic illnesses, medical infrastructure) (Depietri et al., 2013; Knowlton et al., 2009; Mallen et al., 2019). Reid et al. (2009), for instance, identified age, social isolation, and health conditions as key indicators in U.S. census tracts. Environmental factors, both natural (e.g., Land Surface Temperature (LST), vegetation cover) and built (e.g., cooling space access, building density), are also crucial (Song et al., 2020; Hulley et al., 2019). Estoque et al. (2019) highlighted LST and vegetation cover in assessing vulnerability in Philippine cities. However, indicator selection varies regionally due to contextual and data constraints, limiting cross-study comparisons (Li et al., 2022).

The modelling stage of heat vulnerability assessment focuses on developing composite indices, such as the Heat Vulnerability Index (HVI), which integrate various indicators to measure vulnerability across populations or regions. Reid et al. (2009) developed an HVI to identify vulnerable communities and target mitigation efforts. Since then, many HVIs have been introduced globally, including those by Loughnan et al. (2014) and Li et al. (2024c) for Australian cities, Chuang and Gober (2015) and Christenson et al. (2017) for U.S. cities like Phoenix and Milwaukee, and Kitchley (2024) for Madurai, India. A key issue is indicator weighting, as indicators contribute unequally to vulnerability. Methods can be explicit, using equal weights or expert judgement (Guo et al., 2019; Oh et al., 2017), or statistical, employing techniques like Principal Component Analysis (PCA) or the Analytical Hierarchy Process (AHP) (Estoque et al., 2020; Tate, 2012). Equal weighting assumes all indicators are equally important, while PCA groups indicators statistically. Liu et al. (2020) compared these methods in Hangzhou, finding equal weighting better correlated with heat-related mortality. The choice of method significantly affects outputs and depends on the study's context.

Validation is the final and often underdeveloped stage of heat vulnerability assessment, testing model accuracy by comparing outputs to real-world health outcomes, such as heat-related morbidity and mortality (Conlon et al., 2020; Hu et al., 2017; McGeehin & Mirabelli, 2001). Regression methods, including linear and Poisson regression, are commonly used. For instance, Maier et al. (2020) utilised multivariate Poisson regression to assess their HVI model against heat-related deaths in Georgia, while Reid et al. (2009) demonstrated significant correlations between HVI scores and hospital admissions across five U.S. states. Correlation coefficients like Pearson's or Spearman's are also frequently applied; Zhang et al. (2019) validated Chongqing's HVI using high

Pearson correlation coefficients, and Loughnan et al. (2014) used Spearman correlations to validate Australian city-level vulnerability maps. However, validation results often show low agreement between assessed and observed vulnerability (Conlon et al., 2020; Wang et al., 2023; Weber et al., 2015), highlighting the need for more robust methods.

Despite advancements in heat vulnerability research, current studies face several significant limitations. The main issue is the inconsistent use and interpretation of indicators across studies, complicating result comparison and universal application (Li et al., 2022). For instance, the research of Cai et al. (2019) uses only three indicators to assess heat vulnerability, while El-Zein and Tonmoy (2015) incorporate 22 indicators. This significant disparity in the number of indicators illustrates the lack of standardisation, leading to varied assessments of vulnerability. Additionally, Cai et al. (2019) interpret building age as sensitivity and housing price as adaptive capacity, based on the assumption that housing conditions and prices reflect the socioeconomic status of residents. However, this interpretation is weakly supported by existing studies, as it overlooks critical factors like health diversity and demographics, which play a key role in determining vulnerability (Christenson et al., 2017; Loughnan et al., 2014). These variations in indicator selection and interpretation highlight the subjective nature of current heat vulnerability models (Cheng et al., 2021; Li et al., 2022), making it difficult to generalise findings across different regions and contexts.

Additionally, both explicit and statistical weighting methods used to construct these models can introduce biases (Cheng et al., 2021). Explicit weighting, such as equal weights and expert judgment (Guo et al., 2019; Oh et al., 2017), can introduce subjective biases due to human decision-making. This subjectivity is based on experts' opinions or predetermined assumptions about the relative importance of each indicator, which may not accurately reflect their real-world impact. Statistical weighting methods are data-driven but still may fail to fully capture the intricate, non-linear relationships between indicators and heat vulnerability. Validation is a frequently overlooked process, as highlighted by Li et al. (2022). Statistics indicate that two-thirds of current heat vulnerability studies lack validation of their vulnerability results. Among the remaining one-third, many studies show a lack of rigor and thoroughness in the validation of their Heat Vulnerability Models (HVMs), often reporting low correlations between the models' assessments and actual heat vulnerability outcomes. (Conlon et al., 2020; Wang et al., 2023; Weber et al., 2015). This underscores the necessity for more rigorous validation processes (Hulley et al., 2019; Kitchley, 2024; Weber et al., 2015).

Geographical and demographic variability further complicates the application of HVMs. The effectiveness of these models can vary significantly across different regions and populations due to differences in climate, urban infrastructure, and social factors (Oh et al., 2017; Wu et al., 2022). As a result, models developed for one area may not be directly applicable to another. Data availability and accuracy also pose substantial challenges. Reliable data on critical indicators are scarce, particularly in developing regions, which can undermine the accuracy of HVMs (Cheng et al., 2021; Macintyre et al., 2018). While HVMs offer valuable insights for urban planning and public health interventions, their integration into final policymaking is limited because the theoretical potential often faces practical obstacles, such as the complexity of regional differences, data scarcity, and model errors (Cheng et al., 2021). There is a pressing need to bridge the gap between model findings and actionable strategies for heat mitigation and adaptation to ensure that the insights from these studies are effectively translated into real-world applications.

This paper addresses limitations in traditional heat vulnerability studies by integrating machine learning algorithms with multi-source data to enhance model accuracy, applicability, and reliability. Machine learning efficiently processes large, complex datasets and identifies hidden patterns traditional models overlook (Li et al., 2023). For

example, in traffic management, it predicts flow and optimises public transport routes, aiding urban planners in managing dynamic systems (Almukhalfi et al., 2024; Modi et al., 2022). Similarly, in urban heat island studies, machine learning enhances temperature prediction and analysis (Liu et al., 2024; Tanoori et al., 2024) and is widely used to predict air pollutants like PM_{2.5} and NO₂, enabling targeted interventions (Kim et al., 2021; Meng et al., 2018; Tella et al., 2021). By providing accurate, data-driven insights, it supports evidence-based, regionally tailored strategies for urban challenges. Indicator selection inconsistency is mitigated through a systematic review, categorising them into demographic, socioeconomic, health, and environmental factors (Li et al., 2022). Bias in weighting is reduced by deriving relationships directly from data. Advanced algorithms like Random Forest and Gradient Boosting capture non-linear relationships without relying on subjective expert judgment (Chen et al., 2021b; Li et al., 2023; Yang et al., 2022).

This study addresses validation inadequacies in traditional models by implementing rigorous training, cross-validation, and evaluation metrics to ensure generalisability across scenarios. To account for geographical and demographic variability, the models incorporate diverse indicators and are applied across urban contexts in Australian

capital cities. High-quality remote sensing, detailed census data, and extensive points of interest (POIs) enhance spatial and temporal resolution, enabling precise identification of vulnerable areas often overlooked by traditional HVMs due to coarser data (Wang et al., 2023; Wu et al., 2022). These datasets, with their wide coverage and accessibility, are adaptable for large-scale applications. This study further improves traditional HVMs by refining weight allocation and validation processes, addressing issues like inconsistent indicators, weighting biases, and inadequate validation. By validating with real-world data, such as heat-related morbidity and mortality, the results align closely with actual vulnerability patterns (Niu et al., 2021). These enhancements yield robust, fine-scale assessments that provide actionable insights for urban planning and public health, bridging the gap between model outputs and practical applications.

To date, there is a lack of machine learning applications in assessing heat vulnerability. Therefore, the primary objective of this study is to fill this gap by evaluating the effectiveness of various machine learning algorithms in assessing heat vulnerability across Australian capital cities using heat-related indicators. By doing so, the research aims to identify key indicators of heat vulnerability and highlight regional disparities. The findings are expected to inform urban planners and policymakers in

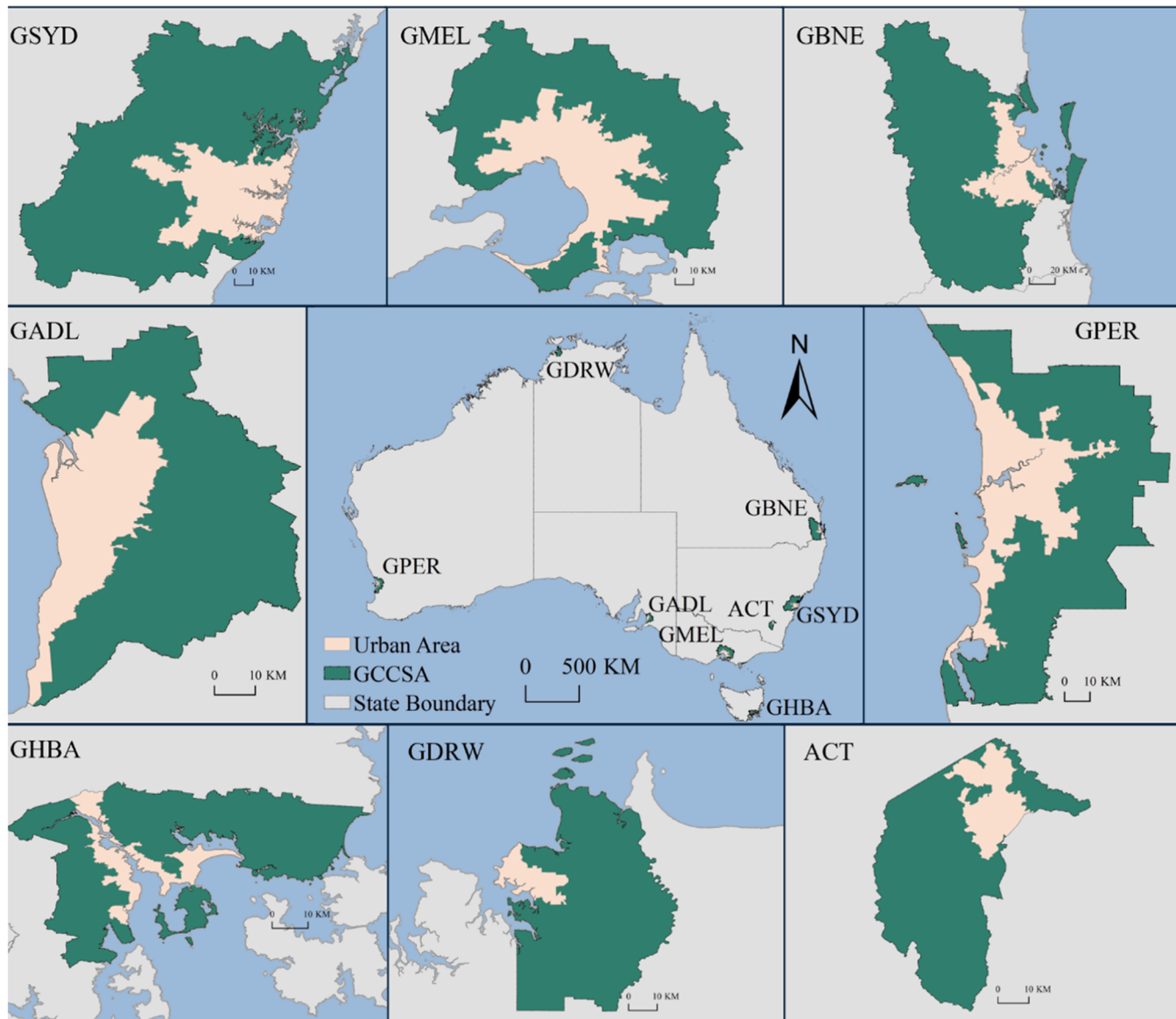


Fig. 1. Study areas: Australian capital cities.

developing targeted mitigation and adaptation strategies, ultimately enhancing urban sustainability and climate resilience. The study's significance lies in its potential to advance the application of machine learning in environmental research and provide actionable insights for improving public health and social equity in urban areas. This ensures more efficient and equitable resource allocation in urban environments.

This paper is structured as follows: [Section 2](#) outlines the study area, methods for model development, evaluation, and heat vulnerability analysis. [Section 3](#) compares machine learning performance, analyses heat vulnerability across cities, and conducts a sensitivity analysis of indicators. [Section 4](#) discusses findings in the context of urban planning and policy interventions, while the conclusion summarises key insights and implications for mitigating heat vulnerability and promoting thermal equity.

2. Research design

2.1. Study area

This study focuses on Australia's eight major metropolitan regions: Greater Sydney (GSYD), Greater Melbourne (GMEL), Greater Brisbane (GBNE), Greater Perth (GPER), Greater Adelaide (PADL), Greater Hobart (GHBA), Greater Darwin (GDRW), and the Australian Capital Territory (ACT) ([Fig. 1](#)). These regions, which are key economic, cultural, and population centres, face increasing heat vulnerability due to urban expansion and climate change (Australian Bureau of Meteorology, 2021). The Australian Census 2021 shows that the capital cities account for about 66.95 % of the total population in all 39,862 Statistical Area Level 1 (SA1 s) (Australian Bureau of Statistics, 2022). The rapid urbanisation in these areas has resulted in extensive hard surfaces, reducing green spaces and water bodies, thereby exacerbating the urban heat island effect (Harmay et al., 2021; Iping et al., 2019; Loughnan et al., 2014). Cities like Sydney and Melbourne experience higher temperatures in their central areas compared to suburban regions (Loughnan et al., 2014; Zhang et al., 2018).

Climate change has intensified this issue, with more frequent and severe heatwaves posing serious health risks to residents, especially vulnerable groups such as the elderly, children, and low-income populations (Chambers et al., 2020; Green et al., 2016). Researching these metropolitan areas' heat vulnerability can help develop effective public health strategies, create fairer urban planning policies, and provide data-driven insights for informed decision-making in urban planning, public health, and environmental protection (Gudes et al., 2010). Australia's metropolitan areas offer rich scenarios for studying heat vulnerability, improving residents' quality of life and health, and providing valuable insights for global regions facing climate change challenges (Yigitcanlar et al., 2022).

2.2. Methodology

A comprehensive framework comprising four major steps—Indicator Selection, Data Collection & Processing, Machine Learning Selection & Development, and Heat Vulnerability Analysis—has been developed to systematically assess heat vulnerability (see [Fig. 2](#)). The Indicator Selection step involves identifying and choosing relevant heat-related indicators based on established population vulnerability and heat risk frameworks. These indicators encompass demographic and socioeconomic characteristics such as age, economic status, social isolation, education level, and population density; health conditions like personal illness status, availability of medical resources, and disability status; and environmental factors including LST, vegetation cover (Normalised Difference Vegetation Index, NDVI), availability of cooling spaces, land cover/use, and building density (Normalised Difference Built-up Index, NDBI). Labelled data, which includes heat-related morbidity and mortality, is crucial in this context as it provides a concrete outcome measure against which the predictive machine learning models can be

trained and validated. This labelled data distinguishes between direct heat-related illnesses and indirect heat-related conditions, allowing for a more nuanced understanding of how different factors contribute to heat vulnerability. By incorporating labelled data, the machine learning models can learn patterns and associations between the indicators and the heat-related health outcomes, thereby enhancing the accuracy and reliability of the assessments.

Data Collection & Processing utilises a variety of sources to ensure a comprehensive and multi-dimensional approach, including remote sensing data from Landsat 8, Sentinel 2, and Digital Earth Australia (DEA); statistical datasets from the Australia Census 2021; and Points of Interest (POI) gathered from Open Street Map. Data processing tools such as Google Earth Engine and ArcGIS Pro are employed to handle operations including data filtering and cleaning, LST, NDVI, and NDBI calculations, kernel density analysis, and data standardisation, conducted at the SA1 scale to facilitate detailed spatial analysis.

In the Machine Learning Selection & Development step, the study employs a selection of machine learning algorithms—Random Forest (RF), Gradient Boosting (GB), Ridge Regression (RR), Linear Regression (LR), XGBoost (XGB), Support Vector Machine (SVM), Multi-Layer Perceptron (MLP), and K-Nearest Neighbors (KNN)—to develop assessment models for heat vulnerability. The process involves model training, validation, and testing using Google Colab, hyperparameter optimisation to enhance model performance, and evaluation using R-Square, Mean Absolute Error (MAE), and Mean Squared Error (MSE) metrics.

The final step, Heat Vulnerability Analysis, involves a comprehensive analysis of heat vulnerability across Australian capital cities through spatial analysis visualising the spatial distribution of vulnerability, statistical analysis quantifying heat vulnerability, and sensitivity analysis assessing the influence of different indicators on the heat vulnerability outcomes. Heat vulnerability is categorised into five levels based on the ranking percentages of the values assessed by the machine learning model with the highest accuracy (RF): Lowest (0–20 %), Low (20–40 %), Medium (40–60 %), High (60–80 %), and Highest (80–100 %) (Wang et al., 2023). The novelty of this framework lies in its integrative approach, combining diverse data sources and advanced machine learning techniques to comprehensively assess and analyse heat vulnerability. Unlike previous studies that may focus on limited indicators or traditional statistical methods, this study leverages the power of remote sensing, extensive demographic data, and machine learning to provide a more accurate and granular analysis of heat vulnerability. This framework addresses the research gap by offering a multidimensional assessment of vulnerability and utilising a robust methodological approach to ensure reliability and precision in the findings.

2.2.1. Indicator selection

Referring to a rigorous and systematic literature review of measures assessing heat vulnerability (Li et al., 2022), this study meticulously selects indicators representing the vulnerability components ([Table 1](#)). The findings were further conceptualised and visualised as a conceptual framework in the study of Li et al. (2024a) (Appendix A). The review employed the PRISMA (Preferred Reporting Items for Systematic Reviews and Meta-Analyses) approach to evaluate and synthesise findings from 76 relevant peer-reviewed articles. The goal of the review was to identify and synthesise methods used to assess urban heat vulnerability. To achieve this, the study established specific inclusion criteria, requiring that the articles be peer-reviewed, published in English, available in full text, and relevant to urban heat vulnerability assessments. The initial search yielded 368 records using keywords such as "urban heat," vulnerab*, and method* from an academic search engine provided by the Queensland University of Technology Library, which offers access to all major databases, including Scopus and Web of Science. After reviewing abstracts and conducting two rounds of full-text screening, 76 peer-reviewed articles were included, all of which were directly relevant to the study's objectives and met the inclusion criteria. The review extracted indicators commonly used in heat vulnerability

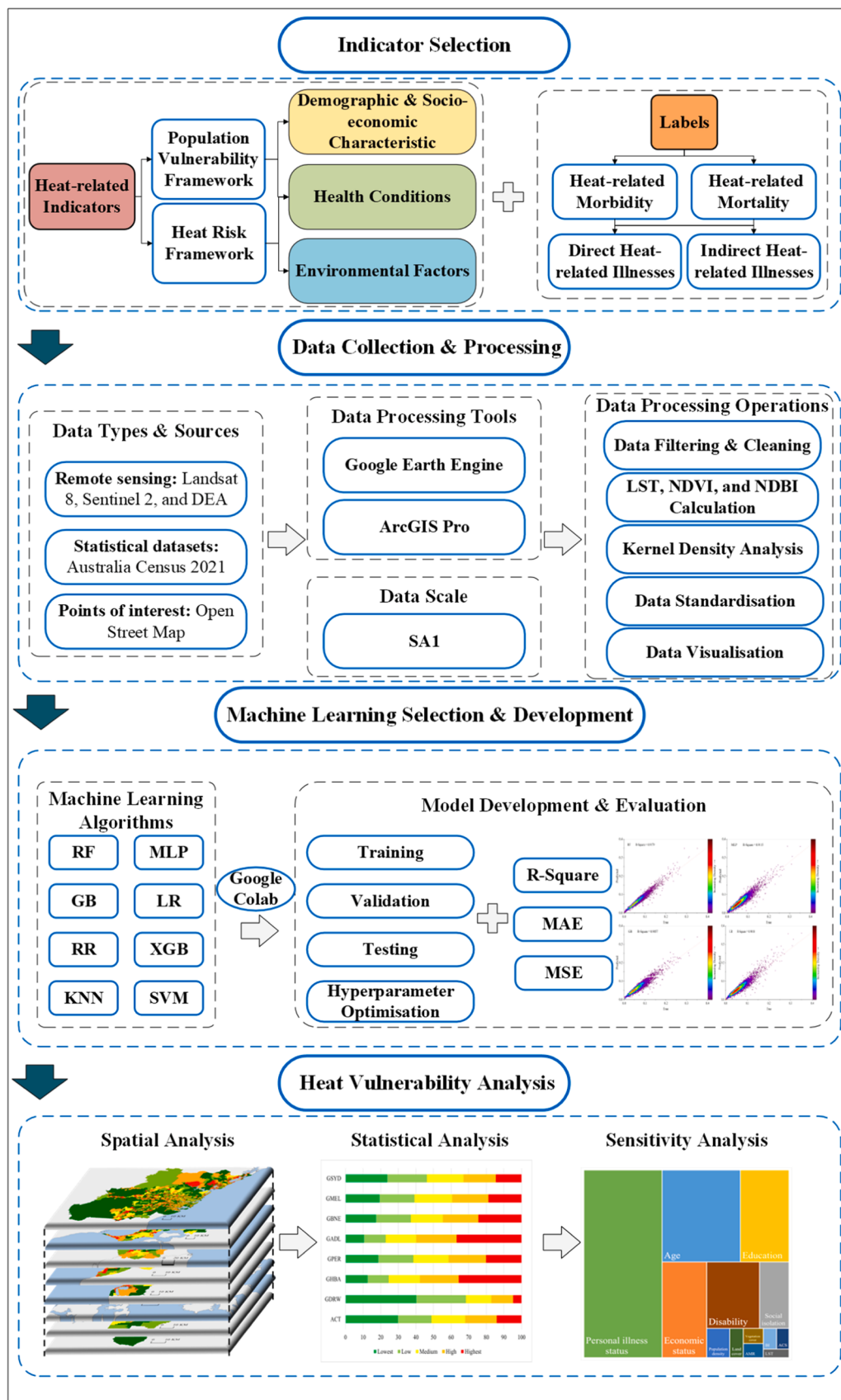


Fig. 2. Research framework.

Table 1

Information of heat vulnerability indicators.

Categories	Indicators	Descriptions	Units	Data Ranges	Vulnerability Elements	Data Source
Demographic and socioeconomic characteristics	Age	Population aged below 5 or over 65	Persons	[0,1535]	Sensitivity	Census 2021
	Economic status	Population with low incomes less than \$800 weekly	Persons	[0,2196]	Sensitivity	Census 2021
	Social isolation	Population living alone	Persons	[0,644]	Sensitivity	Census 2021
	Education	Population with a low education level below Grade 12	Persons	[0,1585]	Sensitivity	Census 2021
Health conditions	Population density	Population density of each SA1	Persons/km ²	[0,158,534]	Sensitivity	WorldPop
	Personal illness status	Population with heat-related long-term physical/mental illness	Persons	[0,2106]	Sensitivity	Census 2021
	Availability of medical resources	Availability to medical resources such as hospital/pharmacy/doctor/chemist	Points/km ²	[0,6.53]	Adaptive Capacity	OpenStreetMap
Environmental factors (natural)	Disability	Population with disability	Persons	[0,525]	Sensitivity	Census 2021
	LST	Daytime LST	°C	[18.11,47.08]	Exposure	Landsat 8
	Vegetation cover	Mean value of NDVI	None	[-1,1]	Adaptive Capacity	Sentinel 2
Environmental factors (built)	Availability of cooling spaces	Availability to public places with free cooling services	Points//km ²	[0,9.25]	Adaptive Capacity	OpenStreetMap
	Land cover/use	Area of developed urban land cover	km ²	[0,13.97]	Sensitivity	Digital Earth Australia
	Building density	Mean value of NDBI	None	[-1,1]	Sensitivity	Sentinel 2

assessments from these articles, re-categorising them into three main groups: demographic and socioeconomic characteristics, health conditions, and environmental factors (both natural and built) (Table 1). This thorough review ensures the representativeness and relevance of the indicators while enhancing general applicability and minimising subjective judgment, thus providing a standard for indicator selection in future heat vulnerability research. Additionally, the study (Li et al., 2024a), which focuses on the development of a standardised and advanced heat vulnerability assessment methodology, further conceptualised and visualised the findings, serving as a conceptual framework (Appendix A).

According to the Intergovernmental Panel on Climate Change, vulnerability is defined by three key elements: exposure, sensitivity, and adaptive capacity (Parry, 2007). Exposure refers to the degree to which a system or population is subjected to the impacts of climate change, such as extreme heat. Sensitivity represents the extent to which a system or group responds to these impacts. Adaptive capacity refers to the ability of a system to cope with, adapt to, and mitigate these impacts. In the context of heat vulnerability, these components interact to determine the overall level of vulnerability to extreme heat, collectively contributing to increased heat-related mortality and morbidity (Li et al., 2024c). The re-categorisation reflects a balanced approach that encompasses various dimensions of heat vulnerability: Demographic and Socioeconomic Characteristics play a crucial role in reflecting the population's sensitivity to heat hazards. Age, which captures the population aged below five or over sixty-five, is a critical indicator due to the increased physiological vulnerability of these age groups to heat-related morbidity and mortality. Economic status, measured by the number of individuals with incomes below \$800 per week (the Australian minimum wage), highlights the financial limitations that impede access to heat mitigation resources. Social isolation, representing individuals living alone, reflects the lack of social support, which increases vulnerability during extreme heat. Education, measured by the population with educational attainment below Grade 12 (excluding higher or vocational education), affects preparedness and awareness of heat risks and appropriate responses. High population density increases anthropogenic heat and exacerbates heat retention, while also placing pressure on access to public resources and infrastructure needed to mitigate heat hazards. In areas with higher densities, residents tend to experience increased sensitivity to exacerbated thermal environments.

Health Conditions focus on the physiological and medical factors

that further contribute to sensitivity or adaptive capacity in the face of extreme heat. Personal illness status, which encompasses the population with long-term heat-related physical or mental illnesses (see Appendix B), captures heightened sensitivity due to pre-existing conditions that impair the ability to withstand heat exposure. Disability similarly reflects an increased sensitivity to heat hazards, as individuals with disabilities often face mobility and healthcare access challenges. Conversely, the availability of medical resources, such as hospitals, pharmacies, doctors, and chemists, plays a vital role in enhancing adaptive capacity by facilitating timely medical interventions during heat events.

Environmental Factors, comprising both natural and built environments, influence the population's exposure, sensitivity, and adaptive capacity to heat. In terms of exposure, LST directly measures heat intensity, with higher temperatures indicating greater exposure to heat. Vegetation cover, represented by the mean value of the NDVI, serves as an indicator of adaptive capacity, as areas with higher vegetation cover experience reduced heat exposure due to cooling effects such as shading and evapotranspiration. In the built environment, the availability of public cooling spaces significantly enhances adaptive capacity, providing vulnerable populations with access to cooling services. Land cover/use, which measures the area of developed urban land, is associated with sensitivity, as is building density, represented by the mean value of the NDBI. Both tend to increase heat retention, reduce ventilation, and exacerbate the urban heat island effect, thereby intensifying the overall sensitivity of urban residents to heat exposure.

Unlike prior research, Li et al. (2022)'s review introduces a novel re-categorisation of indicators into three balanced categories, enhancing clarity and balance for a more comprehensive assessment of heat vulnerability. This approach addresses two critical aspects: the representativeness and comprehensiveness of the indicators, and the mitigation of inconsistencies and biases in their selection. By systematically grouping widely accepted and recently validated indicators (Cheng et al., 2021; Li et al., 2022), the framework ensures up-to-date and methodologically rigorous inputs. This structured categorisation avoids over-reliance on any single type of indicator, supporting a holistic view of vulnerability and enabling more accurate urban planning and public health outcomes. The balance and clarity within the framework not only enhance its robustness but also provide a valuable reference for standardising indicator selection and categorisation in heat vulnerability studies.

2.2.2. Data collection and processing

The demographic, socio-economic, and health data is mainly retrieved from the Australian Census 2021. Only the population density data is obtained from WorldPop with a 100 m resolution. The environmental factors are divided into natural and built indicators, reflecting different dimensions of exposure, sensitivity, and adaptive capacity. Among the natural factors, LST is obtained from Landsat 8 satellite data with a spatial resolution of 30 m, providing an analysis of daytime surface temperature distribution to assess heat exposure in urban areas. Vegetation cover (NDVI), based on Sentinel 2 satellite data with a resolution of 10 m, evaluates the amount of green vegetation, serving as an adaptive capacity indicator by reflecting the role of green spaces in mitigating heat exposure. For the built factors, the availability of cooling spaces is derived from OpenStreetMap POI data, identifying public places offering cooling services (e.g., cooling centres, libraries), which are critical for assessing the community's adaptive capacity during heatwaves. Land cover/use, sourced from Digital Earth Australia with a resolution of 25 m, represents the extent of urban development and serves as a sensitivity indicator to measure the impact of urban construction on heat exposure. Building density (NDBI) is obtained from Sentinel 2 data with a 10-meter resolution, indicating the density and layout of urban buildings. It is used to assess the contribution of buildings to the urban heat island effect, serving as a key measure of heat sensitivity.

In this study, the labelled data encompasses heat-related morbidity and mortality attributable to heat-related illnesses from ABS, either directly or indirectly (Appendix B). The research aggregates heat-related morbidity data at the SA1 level (ABS, 2022) and all-cause mortality data at the Statistical Area Level 2 (SA2) level (ABS, 2023b) from Australian capital cities. Subsequently, it estimates SA2 heat-related mortality data based on state-level death rates from heat-related diseases (ABS, 2023a) and resamples it to the SA1 scale according to the population density (Estoque et al., 2020; Wang et al., 2023) (see Eq. (1) & 2). Ultimately, the mean values of heat-related morbidity and mortality at the SA1 scale are computed to serve as the labelled data for analysis, which ranges from 0 to 0.4 after screening outliers.

$$D_{h,SA1} = D_{a,SA2} \times R_{h,State} \times \frac{P_{SA1}}{P_{SA2}} \quad (1)$$

$$V_{SA1} = \frac{1}{2} (M_{h,SA1} + D_{h,SA1}) \quad (2)$$

Where $D_{h,SA1}$ is the heat-related mortality in SA1 s, $D_{a,SA2}$ is the all-cause mortality in SA2 s, $R_{h,State}$ is the heat-related mortality rate in states, P_{SA1} and P_{SA2} are populations in SA1 s and SA2 s, respectively, V_{SA1} is the heat vulnerability in SA1 s, and $M_{h,SA1}$ is heat-related morbidity in SA1s.

In Australia, SA1 and SA2 are geographic units used by the ABS for census and data collection under the Australian Statistical Geography Standard (ASGS). SA1 is the smallest unit, typically covering areas with a small population and defined by visible or socially relevant boundaries, such as roads or natural features. It allows for detailed analysis of localised demographic, social, and economic characteristics. In contrast, SA2 is a larger geographic area that combines multiple SA1s, representing broader communities like suburbs or small towns. SA2 regions are designed to reflect areas of social and economic interaction and are used for more aggregated analysis, such as healthcare, education, or employment trends. The relationship between SA1 and SA2 ensures that data can be analysed both at a fine-grained local level and a broader community level, enabling comprehensive insights into Australia's population and geography.

To quantify availabilities of medical resources and cooling spaces, this paper utilises Kernel Density Analysis to explore the spatial distribution patterns of medical resources and cooling services from POIs (Eq. (3)). Kernel density analysis smooths the data's discreteness, generating a continuous probability density estimate that aids in the intuitive

understanding of the spatial distribution of resources and services (Yu et al., 2017). It also produces specific density values for each location, thereby enabling further quantitative analysis. By comparing the density values across different areas, researchers can quantitatively evaluate the accessibility and availability of medical resources and cooling services, thus providing a foundation for policy formulation and resource optimisation.

$$\hat{f}(x) = \frac{1}{nh} \sum_{i=1}^n K\left(\frac{x - x_i}{h}\right) \quad (3)$$

Where $\hat{f}(x)$ is the estimated density at point x , n is the number of data points, h is the bandwidth (smoothing parameter), x_i are the data points, K is the kernel function, which is a symmetric, non-negative function that integrates to one.

All the data are pre-processed, calculated, standardised, and visualised at the SA1 scale as continuous values using Google Earth Engine (GEE) and ArcGIS Pro 2.9.1, making them suitable for machine learning operations. The dataset comprises a total of 39,862 data points, please see the data units, ranges, and sources in Table 1. Before training machine learning models, collinearity diagnostics have been conducted by using SPSS 29. The results in Appendix C show that the Variance Inflation Factor (VIF) values for all indicators are below 10, with most being under 5, indicating that the degree of collinearity among the input variables is within an acceptable range (Liu et al., 2022; Zhao et al., 2018). Additionally, nonlinear models such as RF, GB, and KNN are generally robust to the effects of multicollinearity, as they do not depend on the estimation of linear coefficients. Instead, these models prioritise the relative importance of variables, rather than their linear interrelationships. Consequently, the presence of multicollinearity typically exerts minimal influence on their performance and accuracy. An exploratory data analysis using scatter plots was conducted to provide a preliminary understanding of the relationships between various input indicators and the labelled data (see Appendix D). The analysis reveals that personal physiological and health characteristics, such as age, illness status, and disability, are positively associated with heat vulnerability, indicating that individuals with these conditions may face greater risks during extreme heat events. Socio-economic factors, including economic status, education, and social isolation, show more scattered or weaker positive relationships with heat vulnerability. In contrast, there are relatively weak negative correlations between the availability of cooling spaces and medical resources and heat vulnerability, indicating a certain mitigation effect. Environmental characteristics, such as LST, vegetation cover, and building density, appear to moderately correlate with heat vulnerability, while the role of factors like population density and land cover/use remains less clear, potentially indicating non-linear effects. Overall, these initial insights highlight the multifaceted nature of heat vulnerability and suggest the need for more advanced modelling to fully understand these dynamics.

2.2.3. Machine learning algorithm selection and development

This study employs eight machine learning regression algorithms to assess heat vulnerability in Australian capital cities. All the algorithms are running on the Google Collaboratory (Colab) cloud-based platform using Python 3.10.12 and the machine learning library Scikit-learn 1.2.2. These algorithms were chosen because they represent a diverse set of typical and robust methods that have demonstrated high performance across various datasets and tasks in urban studies (Li et al., 2023).

RF and GB, for instance, are known for their ability to handle complex, non-linear relationships and have been broadly used in urban studies to predict environmental phenomena, such as air quality and urban heat islands (Jato-Espino et al., 2022; Yang et al., 2022). XGBoost, with its efficiency and accuracy, has also been widely applied in urban studies for tasks like disaster management and pollution monitoring (Chi et al., 2022; Ghaffarian et al., 2021). Ridge Regression and Linear Regression are traditional methods that have been extensively utilised in

urban health studies to identify key sociodemographic and environmental predictors (Aheto et al., 2021; Kan et al., 2019). SVM is recognised for its robustness in high-dimensional spaces and has been used in urban planning to model urban sprawl and building information identification (Lu et al., 2014; Shafizadeh-Moghadam et al., 2017). MLP, as a type of neural network, excels in capturing intricate patterns in large datasets and has been applied in urban studies for predicting energy consumption and urban land cover classification (Afzal et al., 2023; Zhang et al., 2018). KNN, though simpler, is effective for spatial analysis and has been used in studies mapping urban land cover and building footprints (Karalas et al., 2016; Schlosser et al., 2020).

The selection of these algorithms also allows for a comprehensive comparison with existing literature, where traditional statistical models and simpler machine learning approaches have been predominantly used. However, current heat vulnerability research lacks exploration and application of these machine learning algorithms. This study addresses this gap by applying these advanced algorithms to heat vulnerability research, aiming to explore their effectiveness and provide deeper insights into the underlying factors influencing heat-related health risks. By integrating these advanced algorithms, this study aims to enhance the accuracy and reliability of heat vulnerability assessments, thereby contributing to the growing body of research in urban environmental studies.

The selected algorithms are briefly introduced below.

RF: RF builds multiple decision trees and combines their predictions to improve accuracy and stability. It is robust against overfitting, handles high-dimensional data, and works well with missing values, capturing nonlinear relationships effectively. The ensemble nature of RF makes it suitable for identifying key factors influencing heat vulnerability (Jato-Espino et al., 2022; Wang et al., 2022a). The formula is:

$$\hat{y} = \frac{1}{T} \sum_{t=1}^T h_t(x) \quad (4)$$

where T is the number of decision trees, and h_t is the prediction of the t -th tree.

MLP: MLP is a type of neural network with one or more hidden layers, capable of learning complex function mappings. It has a strong nonlinear modelling capability, making it suitable for handling complex patterns and high-dimensional data in heat vulnerability. However, it requires substantial data and computational resources (Afzal et al., 2023; Zhang et al., 2018). The formula is:

$$\hat{y} = f \left(\sum_{i=1}^n w_i x_i + b \right) \quad (5)$$

where f is the activation function, w_i and b are weights and biases.

GB: GB sequentially adds weak learners, usually decision trees, to improve model performance. It is known for high accuracy and the ability to handle nonlinear relationships effectively. GB's robust performance in high-dimensional and complex data makes it ideal for heat vulnerability regression (Xiao et al., 2021; Yang et al., 2022). The formula is:

$$\hat{y} = \sum_{t=1}^T \alpha_t h_t(x) \quad (6)$$

where α_t is the weight, and h_t is the t -th weak learner.

LR: LR assumes a linear relationship between dependent and independent variables. It is simple, easy to interpret, and computationally efficient, making it suitable for situations with clear linear relationships. However, its ability to handle nonlinear relationships is limited (Kan et al., 2019; Zhao et al., 2022). The formula is:

$$\hat{y} = \beta_0 + \sum_{i=1}^n \beta_i x_i \quad (7)$$

where β_i are the regression coefficients.

RR: RR is a linear regression with a regularisation term that helps mitigate multicollinearity issues. It prevents overfitting and improves model generalisability, performing well in handling high-dimensional data, making it a good choice for heat vulnerability analysis (Aheto et al., 2021; Okumus & Terzi, 2021). The formula is:

$$\hat{y} = \beta_0 + \sum_{i=1}^n \beta_i x_i \quad \text{with} \quad \sum_{i=1}^n \beta_i^2 < \lambda \quad (8)$$

where λ is the regularisation parameter.

XGBoost: XGBoost is an efficient implementation of gradient boosting that enhances performance and accuracy. It handles nonlinear relationships well and is suitable for large-scale datasets. XGBoost's efficiency and robustness make it ideal for complex heat vulnerability data (Chi et al., 2022; Ghaffarian et al., 2021). The formula is:

$$\hat{y} = \sum_{k=1}^K f_k(x), \text{ where } f_k \in F \quad (9)$$

Where F is the space of regression trees.

KNN: KNN makes predictions based on the distance between data points. It is simple and non-parametric, suitable for small datasets. However, it relies heavily on data distribution, making it more applicable to cases with clear local patterns in heat vulnerability (Karalas et al., 2016; Schlosser et al., 2020). The formula is:

$$\hat{y} = \frac{1}{k} \sum_{i=1}^k y_i \quad (10)$$

where y_i are the labels of the k nearest neighbours.

SVM: SVM finds the optimal hyperplane in high-dimensional space for classification and regression. It handles high-dimensional data well and has good generalisation ability, though it is computationally intensive. SVM is suitable for small samples and complex data structures in heat vulnerability analysis (Lu et al., 2014; Shafizadeh-Moghadam et al., 2017). The formula is:

$$\hat{y} = w^T \phi(x) + b \quad (11)$$

where $\phi(x)$ is a nonlinear mapping function.

Hyperparameter Optimisation

During the hyperparameter optimisation process, this study partitioned the data into 70 % for training and 30 % for testing. This study employed a manual grid search method for hyperparameter tuning, utilising 5-fold cross-validation for validation (Fan et al., 2024). Specifically, this study defined a grid of potential hyperparameters and applied 5-fold cross-validation, dividing the training data into 5 subsets. In each iteration, 4 subsets were used for training and 1 for validation. This process was repeated for each combination of hyperparameters, with performance metrics recorded at each step. The optimal hyperparameter combination was selected based on cross-validation results, ensuring the model's best performance and generalisation capability. The detailed hyperparameter combinations, learning curves, and optimal results are presented in Appendices E and F.

Performance Evaluation Metrics of Machine Learning Algorithms

This study uses the coefficient of determination (R^2), mean squared error (MSE), and mean absolute error (MAE) as metrics to evaluate the performance of machine learning algorithms in assessing heat vulnerability. These metrics are selected because they provide a balance between measuring model fit and prediction error, ensuring a comprehensive evaluation of both model accuracy and precision (Wang et al., 2022b; Zhou et al., 2024). Additionally, they are widely recognised and commonly used performance evaluation metrics in urban studies that utilise machine learning, making them appropriate for this context (Gao et al., 2023; Kokkinos et al., 2021; Palaniyappan & Vinoprabha, 2024).

R^2 represents the proportion of variance in the dependent variable that is predictable from the independent variables. The closer the value is to 1, the better the model's explanatory power. The formula is as follows:

$$R^2 = 1 - \frac{\sum_{i=1}^n (y_i - \hat{y}_i)^2}{\sum_{i=1}^n (y_i - \bar{y})^2} \quad (12)$$

where y_i are the actual values, \hat{y}_i are the predicted values, and \bar{y} is the mean of the actual values.

MSE measures the average of the squares of the errors between predicted and actual values. A lower MSE indicates higher prediction accuracy. The formula is:

$$MSE = \frac{1}{n} \sum_{i=1}^n (y_i - \hat{y}_i)^2 \quad (13)$$

MAE measures the average of the absolute differences between predicted and actual values. A lower MAE indicates lower prediction error. The formula is:

$$MAE = \frac{1}{n} \sum_{i=1}^n |y_i - \hat{y}_i| \quad (14)$$

By calculating and comparing these metrics, we can comprehensively evaluate the performance of different machine learning algorithms in assessing heat vulnerability. Their combination allows us to evaluate model performance from multiple perspectives, ensuring that both high accuracy and minimal errors are achieved, which is crucial for assessing the spatial distribution of urban heat vulnerability. This, in turn, provides data support and scientific basis for urban planning and policy formulation.

Fig. 3 illustrates how machine learning models are developed to assess heat vulnerability, enhancing the reader's understanding. It begins with data pre-preparation, where various data types, including remote sensing, statistical, and POI data, are processed into continuous values suitable for machine learning regression. This ensures that all inputs are standardised and ready for use in model training. Next, the processed data is fed into the model as inputs, with indicators such as

age, personal illness status, and LST forming the basis for assessing heat vulnerability. These inputs represent different perspectives influencing heat vulnerability. Machine learning algorithms, such as RF and GB, are employed to learn patterns and associations between these input indicators and the labelled data, which, in this case, are heat-related morbidity and mortality. The labelled data serve as the target variable that guides the model's learning process, allowing it to understand the relationships between the inputs and the health outcomes. During model training, the input data is split into training and testing sets, and techniques such as hyperparameter optimisation and cross-validation are applied to refine the model's performance. This step ensures that the models can generalise well to new data and accurately predict outcomes. Once the models are trained, their performance is evaluated using metrics such as R^2 , MAE, and MSE to assess how well the models assess heat vulnerability. The final output of the machine learning process includes heat vulnerability predictions and feature importance rankings. These outputs not only map areas most vulnerable to heat but also provide insights into which variables are the most significant contributors to vulnerability.

2.2.4. Heat vulnerability analysis

The Heat Vulnerability Analysis step involves a comprehensive evaluation of heat vulnerability across Australian capital cities using a multi-dimensional approach. This process integrates spatial, statistical, and sensitivity analyses to assess heat vulnerability in a systematic and robust manner.

Spatial Analysis: Spatial analysis is conducted using ArcGIS Pro 2.9 to map and visualise the geographical distribution of heat vulnerability across different SA1 units. This step helps to capture the spatial variability of vulnerability and identify potential hot spots. The visual representation of heat vulnerability supports further analysis and provides a clear geographic context for understanding the spatial distribution of heat vulnerability in both urban and suburban areas.

Statistical Analysis: To quantify heat vulnerability, the heat vulnerability values assessed by the machine learning model with the highest accuracy (RF) are categorised into five distinct levels based on the ranking percentages: Lowest (0–20 %), Low (20–40 %), Medium

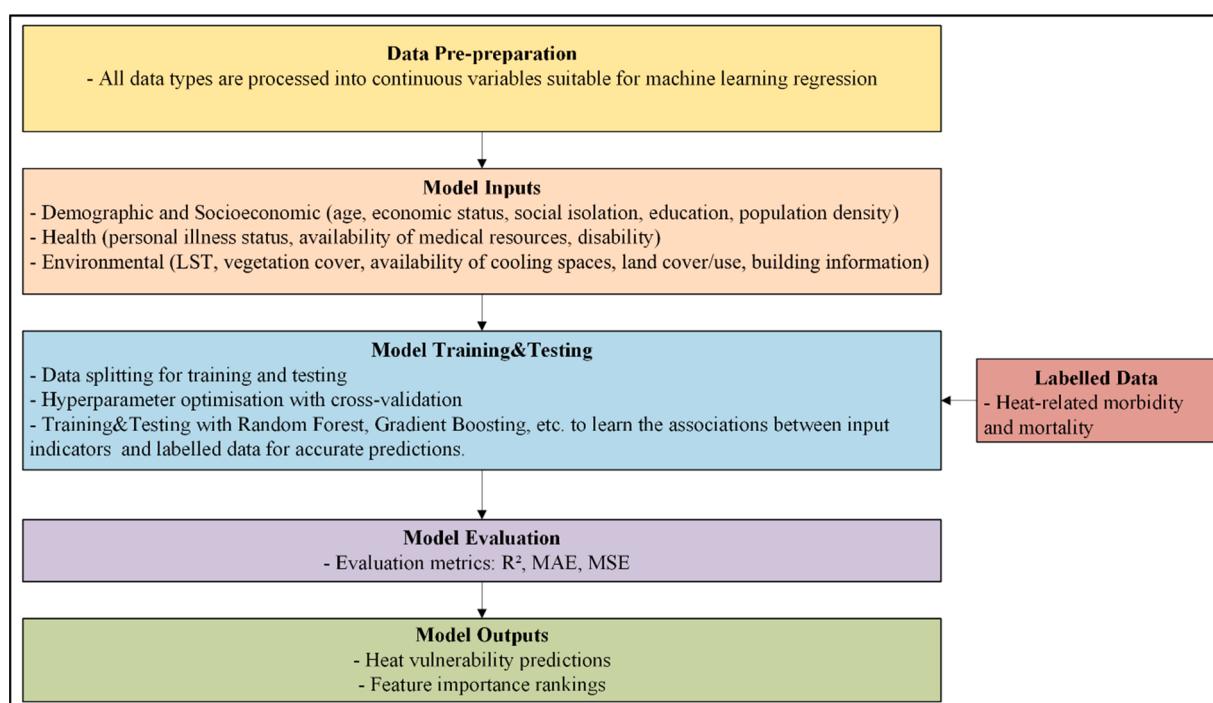


Fig. 3. Workflow of Machine Learning Development.

(40–60 %), High (60–80 %), and Highest (80–100 %) (Wang et al., 2023). The statistical analysis is used to compute the distribution of SA1 units across these vulnerability levels in eight cities. This allows for a comparative assessment of regional disparities, helping to understand the distribution of vulnerability across various geographic areas and providing a structured way to assess which regions may require targeted interventions.

Sensitivity Analysis: Sensitivity analysis is conducted using feature importance rankings derived from the RF algorithm, Partial Dependence Plots (PDP), and SHapley Additive exPlanations (SHAP). This approach identifies the demographic, socioeconomic, health, and environmental factors that contribute most significantly to heat vulnerability. Feature importance offers a global evaluation of each feature's contribution to the model. PDPs aid in interpreting feature importance by visualising the average effect of individual features, while SHAP values provide a more granular insight into how specific features influence individual assessments, ensuring both local and global interpretability (Liao et al., 2024). By combining these techniques, the sensitivity analysis yields insights into the interaction of various variables and their impact on vulnerability, informing the refinement of vulnerability models and policy strategies.

By combining spatial, statistical, and sensitivity analyses, this approach ensures a comprehensive evaluation of heat vulnerability and supports the development of targeted strategies for urban planning and public health.

3. Analysis and results

3.1. Comparative performance of machine learning algorithms

This study evaluated eight machine learning algorithms to assess heat vulnerability in Australian capital cities, focusing on assessment accuracy and error metrics (Table 2, Fig. 4& Appendix G). The RF algorithm emerged as the best performer, achieving R^2 values of 0.9179 (training) and 0.9089 (testing), with MAE of 0.0051 (training) and 0.0076 (testing), and MSE of 0.0001 for both sets. These metrics highlight RF's ability to effectively model complex relationships in the data, making it suitable for visualising the spatial distribution of heat vulnerability in Section 3.2. The MLP also performed well, with R^2 values of 0.9115 (training) and 0.9014 (testing), and similar MAE and MSE values to RF. GB showed slightly lower but reliable performance, with R^2 of 0.9057 and 0.8962. LR and RR had almost identical results, both achieving R^2 values around 0.902, with MAE and MSE values of 0.0078 and 0.0001. XGBoost had slightly lower accuracy, with R^2 values of 0.8842 and 0.8782, but still demonstrated adequate assessment power. KNN showed moderate performance with R^2 values of 0.8613 (training) and 0.8544 (testing) and a slightly higher error. The SVM algorithm performed the worst, with R^2 values of 0.8381 and 0.8343, indicating limited effectiveness in this context. Overall, Random Forest proved to be the most effective algorithm for heat vulnerability assessment, providing key insights for future research and urban heat management.

Table 2
Training and testing accuracy results of machine learning algorithms.

ML Algorithms	Training Accuracy			Testing Accuracy		
	R2	MAE	MSE	R2	MAE	MSE
RF	0.9179	0.0051	0.0001	0.9089	0.0076	0.0001
MLP	0.9115	0.0075	0.0001	0.9014	0.0078	0.0001
GB	0.9057	0.0080	0.0001	0.8962	0.0082	0.0001
LR	0.9018	0.0078	0.0001	0.9050	0.0078	0.0001
RR	0.9017	0.0078	0.0001	0.9049	0.0078	0.0001
XGBoost	0.8842	0.0084	0.0002	0.8782	0.0087	0.0002
KNN	0.8613	0.0082	0.0002	0.8544	0.0094	0.0002
SVM	0.8381	0.0111	0.0002	0.8343	0.0108	0.0002

3.2. Spatial and statistical analysis of heat vulnerability

Heat vulnerability in Australian capital cities is categorised into five levels based on assessments from the RF algorithm, selected for its high accuracy. Fig. 5 shows the spatial distribution of heat vulnerability across eight major Australian capital cities, revealing significant regional disparities and distinct urban characteristics.

GSYD: Heat vulnerability in GSYD displays a clear gradient, with the highest levels in densely populated inner-city areas (red and orange zones). Middle zones show moderate vulnerability (yellow and light green), with some pockets of high vulnerability. The outer suburbs and rural regions (dark green) have the lowest vulnerability, though isolated areas of higher vulnerability can still be found in the middle and northeastern coastal suburbs.

GMEL: In GMEL, heat vulnerability decreases outward from the city centre. The highest vulnerability is found centrally, with gradual decreases in the inner suburbs. The northwestern and southwestern regions have moderate to high vulnerability, while the outer suburban areas have the lowest.

GBNE: GBNE exhibits considerable variation in heat vulnerability. The northern areas are predominantly highly vulnerable, while the central region has lower vulnerability. The eastern coastal region shows elevated vulnerability, particularly in the southern part, while the southern areas generally have lower vulnerability.

GADL: GADL shows an urban-rural gradient, with high vulnerability concentrated in central and southwestern urban areas. Moderate vulnerability appears in central and southeastern regions, while low vulnerability is prevalent in the northern and northeastern suburbs and rural areas.

GPER: In GPER, lower heat vulnerability is seen in coastal and suburban areas, while the urban core experiences higher vulnerability. Inland areas have heterogeneous vulnerability.

GHBA: GHBA shows significant variation, with high vulnerability in central urban areas, lower vulnerability in peripheral suburban and coastal regions, and mixed levels in inland areas.

GDRW: Heat vulnerability in GDRW forms a distinct gradient, with high vulnerability in southern and central regions, surrounded by moderately vulnerable buffer zones. The northern areas have low vulnerability.

ACT: In ACT, high vulnerability is concentrated in the northern and central regions, surrounded by moderately vulnerable areas. The southern and peripheral areas have the lowest vulnerability, illustrating a gradient from high in the densely populated north and central regions to low in less populated southern areas.

In summary, high heat vulnerability is common in the central business districts and inner suburbs of six major cities, including GSYD, GMEL, GBNE, GADL, GPER, and GHBA. These areas are characterised by high population density, extensive impervious surfaces, and limited green space, contributing to the urban heat island effect. In contrast, peripheral and suburban areas have lower vulnerability, benefiting from greater vegetation cover, lower population density, and natural cooling effects like parks and coastal breezes, particularly in Melbourne's eastern suburbs and the coastal areas of Brisbane and Perth. Rural and outlying regions, such as in GDRW and ACT, show the lowest vulnerability, with abundant green zones and minimal urban development. Unique regional patterns also emerge, such as higher vulnerability in northern GHBA's middle part and a balanced vulnerability distribution in Perth's western coastal and central areas. These findings underscore the complex interplay of socio-economic factors, urban density, land use, and natural features in shaping heat vulnerability. Tailored mitigation and adaptation strategies are essential to address local needs and enhance urban resilience to rising heat risks.

The comparative analysis of heat vulnerability across eight major Australian capital cities reveals significant regional differences in the distribution of SA1 units across vulnerability categories. Fig. 6 shows that ACT and GDRW have the highest proportions of SA1 units in the

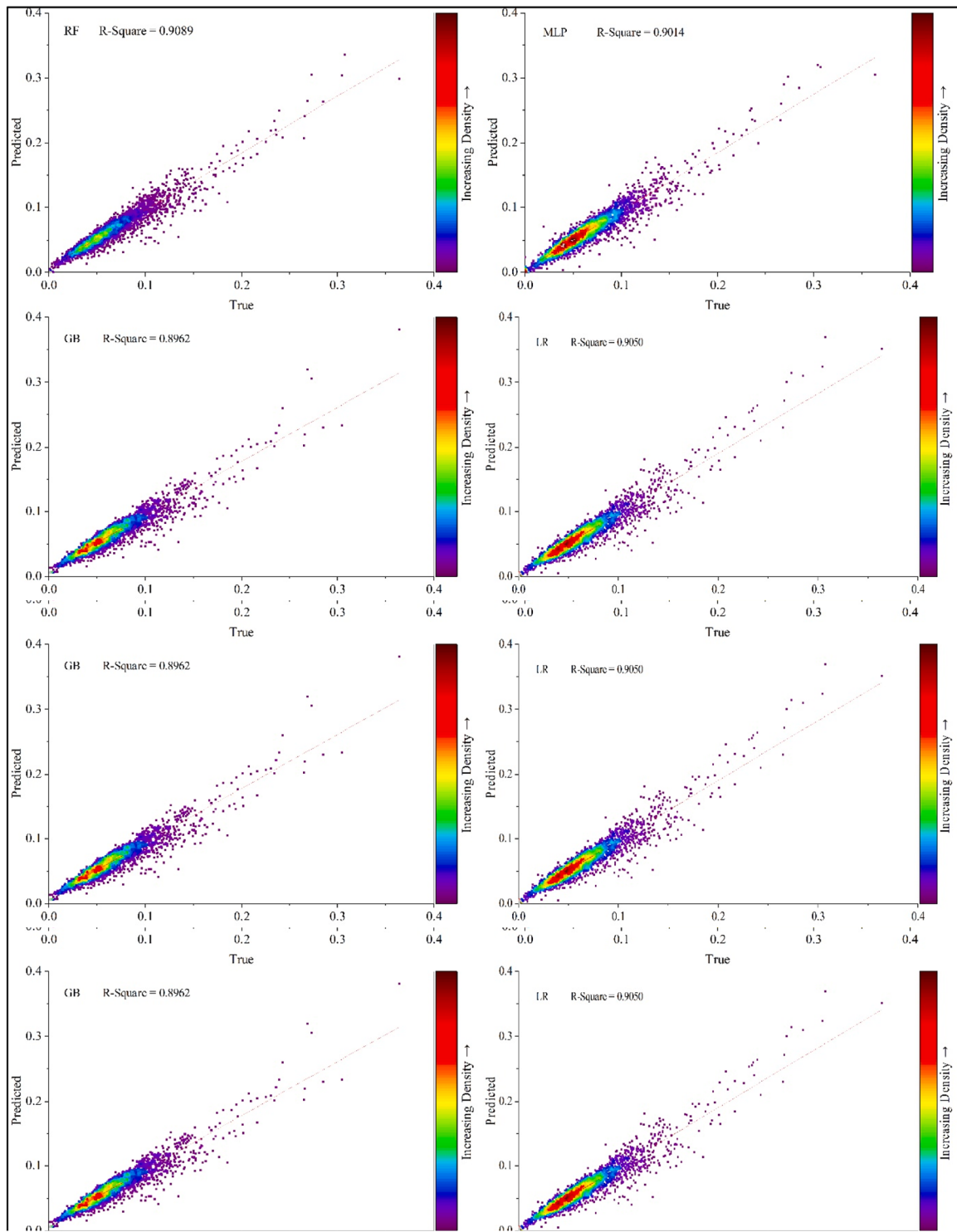


Fig. 4. Testing results of the selected machine learning algorithms.

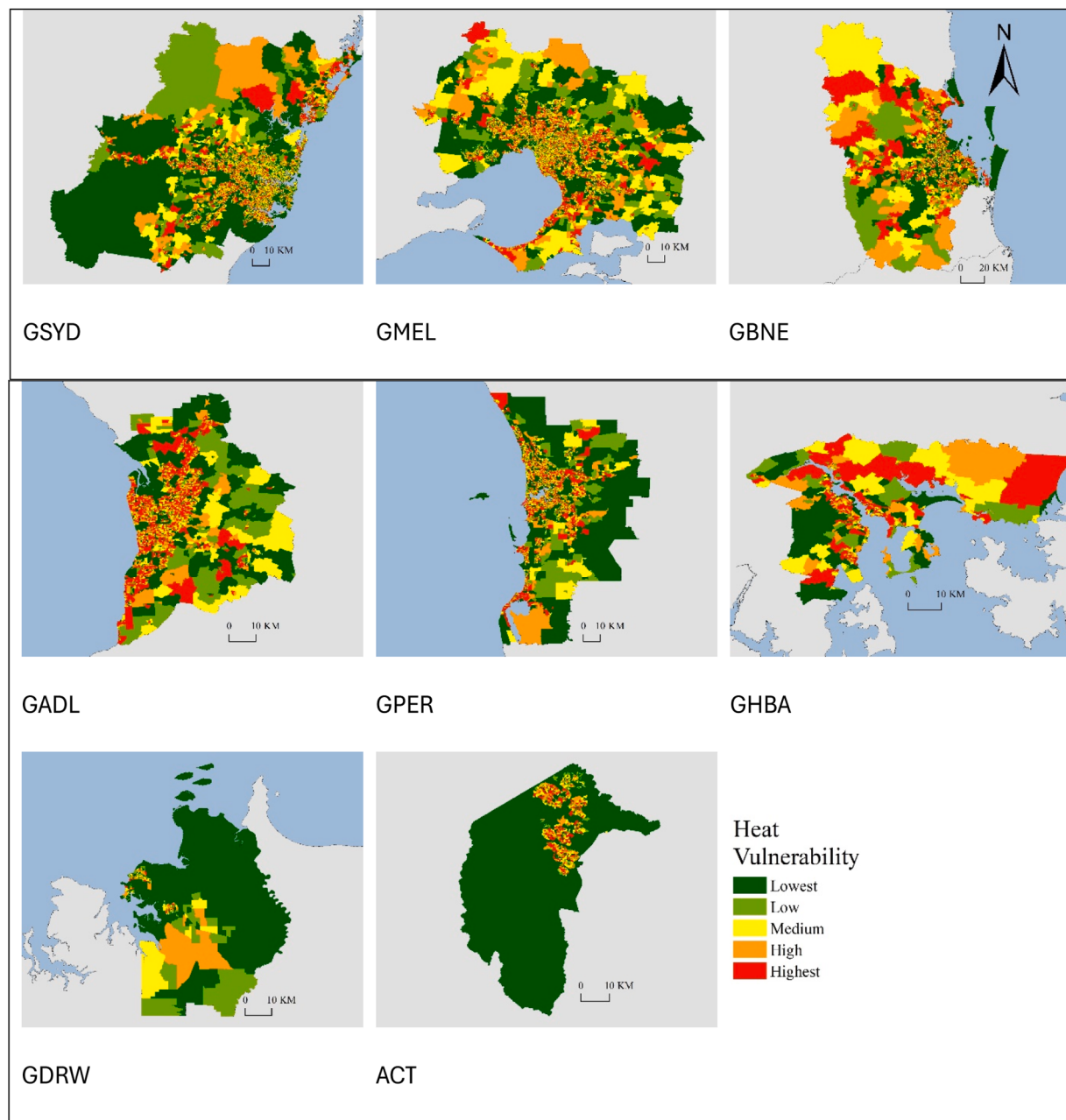


Fig. 5. Spatial distribution of assessed heat vulnerability from RF at the SA1 scale in Australian capital cities.

lowest vulnerability category, at 29.83 % and 40.28 %, respectively, indicating generally lower vulnerability in these areas. In contrast, GHBA and GADL have the largest proportions of SA1 units in the highest vulnerability category, at 35.64 % and 36.91 %, highlighting significant heat vulnerability concerns. GPER, GMEL, and GSYD show more balanced distributions across all categories, indicating diverse vulnerability profiles. GBNE also has a relatively even distribution, with a slight bias towards higher vulnerability. These results underscore the differing levels of heat vulnerability across Australian capital cities, highlighting the importance of region-specific mitigation and adaptation strategies.

3.3. Sensitivity analysis

The sensitivity analysis results, using three interpretability techniques (Fig. 7 & Appendix H)—feature importance treemap, PDP, and mean SHAP values—collectively underscore the role of each heat-related indicator in determining heat vulnerability. As highlighted by

both visualisations and SHAP value assessments, personal illness consistently emerges as the most influential factor. The treemap identifies it as the largest segment, while the SHAP values further confirm this, showing the highest mean value (0.0136) and a positive trend in the PDP. This suggests that individuals with chronic health conditions are particularly susceptible to heat stress, a finding of significant concern for public health interventions. In addition to illness status, age and education also rank highly in both analyses. The treemap demonstrates their notable contributions, with the elderly and very young populations being especially vulnerable, likely due to physical frailty and reduced ability to regulate body temperature. Similarly, the PDP for age displays a strong positive trend, with a SHAP value of 0.0045, confirming its substantial impact. Education, while slightly less influential than age and illness, still plays a significant role. Lower educational attainment is linked to higher vulnerability, likely due to a lack of heat risk awareness and fewer resources available for mitigation. Economic status and social isolation also feature prominently, albeit with somewhat lower SHAP

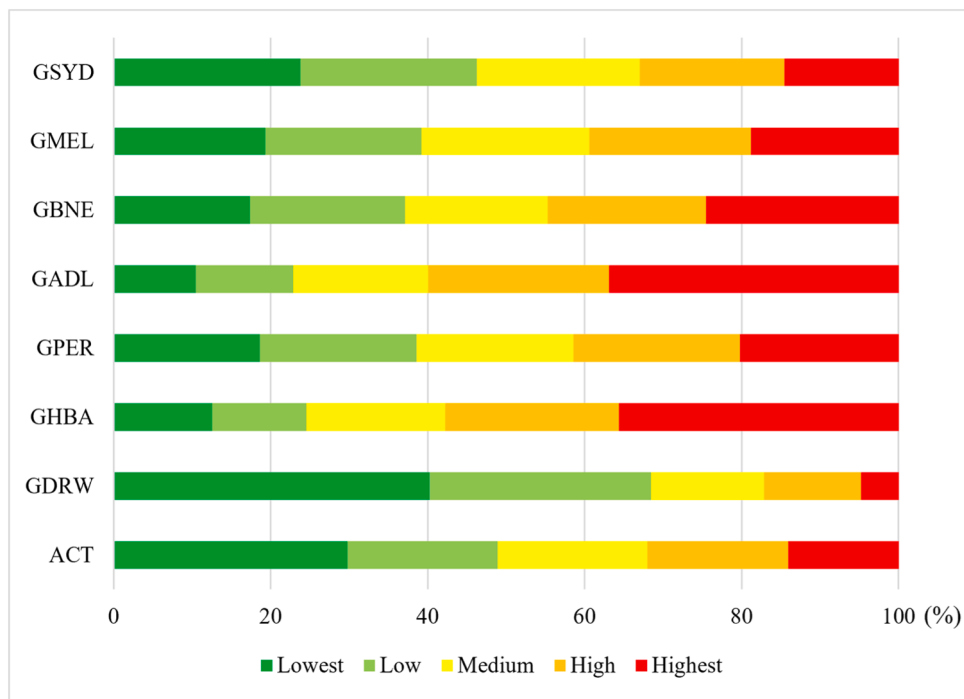


Fig. 6. Proportions of SA1 s in heat vulnerability levels across Australian capital cities.

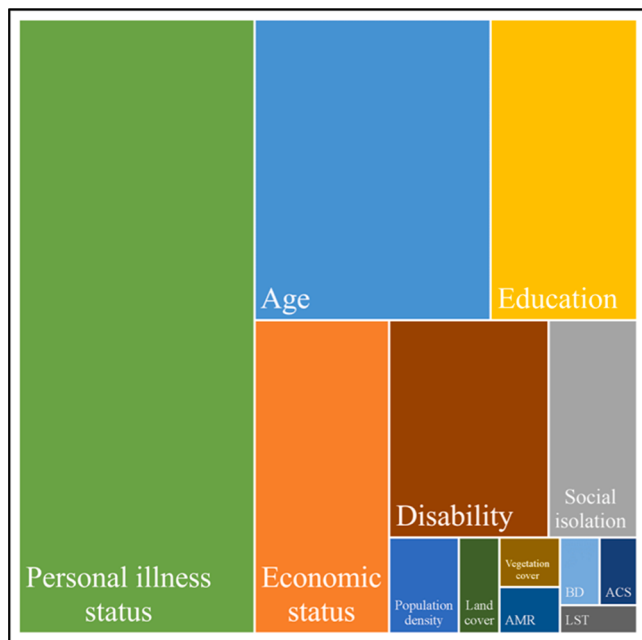


Fig. 7. Treemap of feature importance for heat-related indicators in Australian capital cities. Notes: ACS for availability for cooling spaces; AMR for availability for medical resources; BD for building density.

values (ranging from 0.0019 to 0.0026). Both the treemap and SHAP analyses suggest that these variables contribute to vulnerability by limiting access to cooling resources, healthcare, and social support. The influence of disability follows a similar pattern, with moderate but meaningful contributions to the model's assessments, further highlighting the importance of socioeconomic and demographic factors. Other indicators, primarily environmental and infrastructural, exhibit smaller SHAP values and appear as minor segments in the treemap. Population density and the availability of medical resources, for

instance, have smaller SHAP values, indicating limited contribution to the model. Although their PDPs show some level of influence, particularly at lower values, their overall effect diminishes as their values increase. LST, vegetation cover, availability of cooling spaces, land cover, and building density also display minimal SHAP values, suggesting their marginal role in the model's outcomes. The PDP trends further support this, with some factors showing negative or fluctuating effects, reinforcing their limited relevance to the assessments. While these environmental and infrastructural factors play a role, their contribution to heat vulnerability is significantly overshadowed by health and socio-demographic variables. These findings underscore the complex interplay between individual health, social conditions, and the physical environment, with personal health and demographic characteristics emerging as the most critical determinants of heat vulnerability.

4. Findings and discussion

The study successfully utilised eight machine learning algorithms to assess heat vulnerability in Australian capital cities, revealing several critical insights. The RF algorithm emerged as the most robust model, with R^2 values of 0.9179 for the training set and 0.9089 for the testing set, underscoring its superior ability to capture complex relationships within the data. Spatial analysis revealed significant regional disparities, with higher heat vulnerability in densely populated urban centres and areas with limited green spaces, while suburban and rural regions with higher vegetation cover exhibited lower vulnerability. This highlights a substantial imbalance in heat vulnerability between urban and suburban areas. Notably, the ACT and GDRW have the lowest proportions of highly vulnerable SA1 units, whereas GHBA and GADL show the highest, indicating significant regional disparities that necessitate tailored heat mitigation strategies. Sensitivity analysis revealed that personal health conditions and sociodemographic characteristics, such as personal illness status, age, and education level, play dominant roles in determining heat vulnerability, overshadowing the impact of environmental and infrastructural factors.

The study's findings can be attributed to several key factors. The superior performance of the RF algorithm is likely due to its ability to handle complex, nonlinear relationships and interactions among the

various heat vulnerability indicators. This algorithm's ensemble approach combines multiple decision trees, effectively capturing intricate patterns in the data that simpler models might miss (Belgiu & Drăguț, 2016; Ye et al., 2019). From the most evident environmental differences, the significant regional disparities in heat vulnerability can be explained by the varying urbanisation levels, population densities, and green space availability across different cities (Chen et al., 2018). Densely populated urban centres with extensive impervious surfaces and limited vegetation exacerbate the urban heat island effect, leading to higher heat exposure (Wang et al., 2023). Conversely, suburban and rural areas benefit from greater vegetation cover, which provides natural cooling and reduces heat exposure (Li et al., 2024b). However, the sensitivity analysis reveals that personal health conditions and socio-demographic characteristics—such as illness status, age, and education—play a more dominant role in determining individual vulnerability. The dominance of personal health conditions and socio-demographic characteristics in determining heat vulnerability aligns with the theoretical framework of social determinants of health, which posits that an individual's social and economic conditions significantly influence their health outcomes (Marmot, 2005; Solar & Irwin, 2010). Populations with chronic health conditions, the elderly, and those with lower education levels are less capable of coping with heat stress, making them more vulnerable. This finding supports existing models that emphasise the importance of addressing social inequalities to mitigate health risks.

When comparing this study's results with existing literature, several key points of convergence and divergence emerge. Previous research has consistently shown that urban centres with high population densities and limited green spaces tend to exhibit higher heat vulnerability due to the urban heat island effect (Aubrecht & Özceylan, 2013; Li et al., 2024c; Wang et al., 2023). This study's findings align with these observations, reinforcing the notion that urbanisation significantly impacts heat exposure and vulnerability. Moreover, the emphasis on sociodemographic factors such as age, health conditions, and education level as primary determinants of heat vulnerability is well-supported by existing models of social determinants of health (Marmot, 2005). This study advances the understanding of heat vulnerability by integrating machine learning algorithms, thereby enabling a more precise and refined identification of key vulnerability indicators. Comparative studies on Australian capital cities provide valuable context for evaluating the performance of different approaches. Loughnan et al. (2014), for instance, developed a heat vulnerability index for Australian capital cities, employing stepwise linear regression for weighting and validating their index using Spearman correlation coefficients against emergency service demand during extreme heat events. Their findings indicated accuracy levels ranging from 0.186 to 0.807, with the majority of cities achieving accuracy below 0.60. Similarly, Wang et al. (2023) proposed a heat health risk index for Australian capital cities, utilising equal weighting and principal component analysis, and validated the index using hospital admissions, deaths, and death rates during summer periods. However, their Pearson correlation coefficients between index values and validation variables were all below 0.1, suggesting weak linear relationships. More recently, Li et al. (2024c) introduced a comprehensive heat vulnerability index, incorporating more representative and balanced indicators same to this study, and adopting a weighting approach referring to Wang et al. (2023). Their index was validated against heat-related deaths, yielding Pearson correlation coefficients of 0.92 and 0.68 for deaths estimated by population and death causes at the SA2 scale, corresponding to R^2 values of approximately 0.85 and 0.46 in linear models. In contrast, machine learning-based heat vulnerability models in this study demonstrated superior assessment performance, with R^2 values consistently exceeding 0.83 in both training and testing phases. Notably, the RF algorithm achieved R^2 values above 0.90, highlighting its robustness and accuracy. This comparison underscores the enhanced precision offered by machine learning approaches, particularly RF, in assessing heat vulnerability, thereby

reinforcing the potential of these advanced analytical techniques in improving vulnerability assessments.

Traditional methods such as equal weighting and PCA, the two most frequently used methods, are limited in accurately demonstrating how indicators influence heat vulnerability. Equal weighting assumes that all indicators contribute equally, which overlooks the fact that different indicators may have varying levels of impact. It also fails to capture interactions between indicators, which can significantly affect outcomes. For example, Christenson et al. (2017) assigned equal weights to a total of 23 vulnerability indicators, such as air surface temperature, air quality, and poverty rate. While air quality can exacerbate heat vulnerability by contributing to higher temperatures through pollutants like ozone, air surface temperature has a more immediate and direct effect on thermal stress and heat-related health risks. Similarly, poverty exerts a more pervasive influence than the proportion of households without a vehicle, as it not only limits access to air conditioning and healthcare but also affects housing quality and insulation, further increasing heat exposure. Furthermore, although diabetes prevalence is recognised as a major risk factor for heat-related morbidity, it is less directly associated with heat-induced outcomes than heat stress, which represents a more immediate and universal health threat during extreme heat events. PCA, while useful for reducing dimensionality, compromises interpretability by transforming original indicators into principal components, which are difficult to relate back to the specific factors driving vulnerability. For instance, in the research of Hulley et al. (2019), the green vegetation fraction is grouped into a component with income and education, which is interpreted as representing adaptability through socioeconomic status, despite vegetation being more closely related to environmental factors than to socioeconomic adaptability. Similarly, the elderly population is included in a component with population density and building height, labelled as representing sensitivity through urban congestion, even though the elderly population has no direct contribution to urban congestion compared to the other two indicators. Moreover, PCA does not account for the relationship between indicators and the target variable, making it less suited for understanding direct influences on heat vulnerability. This study adopts an integrated approach combining feature importance, PDP, and SHAP values to explore the influence of heat-related indicators on heat vulnerability and to enhance result interpretability (Liao et al., 2024). Feature importance provides an overall evaluation of each feature's contribution, while PDP reveals the marginal effect of individual features. SHAP values explain the contributions of features at the individual level. Together, these methods offer a comprehensive understanding of feature influence from global, marginal, and individual perspectives. This methodological innovation challenges traditional approaches that rely on simpler statistical models, suggesting that machine learning can provide deeper insights into the complex interplay of factors influencing heat vulnerability.

The methodological framework utilised in this study advances existing heat vulnerability assessment practices in terms of indicator selection, weight allocation, and result validation. This study adopts the theoretical framework for indicator selection and categorisation proposed by Li et al. (2020), which incorporates widely accepted and representative indicators re-categorised into balanced groups. The high accuracy of the results demonstrates that this study provides a solid empirical validation of the indicator framework, helping to address limitations in current studies by providing standardised and comprehensive indicator references. Existing studies lack a standard for indicator selection, leading to inconsistent indicator use and interpretation. For instance, the number of indicators used varies significantly, such as three indicators selected in Cai et al. (2019)'s study compared to 22 indicators utilised in El-Zein and Tonmoy (2015)'s work. Subjective indicator selection also exists; for example, Prosdocimi and Klima (2020) used access to sewage and garbage services to assess heat vulnerability, which is rarely used and lacks supporting references. Traditional HVMs typically rely on explicit methods (such as equal

weights and expert judgment) (Guo et al., 2019; Oh et al., 2017) or statistical techniques (such as PCA and AHP) (Estoque et al., 2020; Tate, 2012) to determine the weight of each indicator, which can introduce subjective biases and make it difficult to capture the non-linear relationships between indicators and heat vulnerability. In this study, machine learning algorithms are used to automatically learn the relationships directly from multi-dimensional data, reducing biases introduced by human subjectivity and statistical limitations, thereby making the weight assignment more objective and accurate. A lack of validation processes and low validation accuracy are other key limitations in existing studies. Reviews reveal that only 25 % of reviewed studies involved validation processes, and validation results varied significantly. For example, the R^2 value between assessed heat vulnerability and observed deaths was less than 0.01 in Conlon et al. (2020), and only 0.32 in Kim et al. (2017). This study addresses this by involving heat-related morbidity and mortality as labelled data and implementing strict validation methods, such as cross-validation and test set evaluation, thereby improving the accuracy and reliability of the assessment results. Moreover, this framework comprehensively evaluates heat vulnerability by integrating remote sensing data, detailed census data, and POI information. These multi-source data not only enhance the spatial and temporal resolution of vulnerability assessments, enabling more accurate identification of vulnerable areas that traditional HVMs may overlook due to coarse data but also improve the applicability of models across different geographic and demographic contexts.

The unique contribution of this research lies in its comprehensive application of machine learning to assess heat vulnerability, coupled with the use of diverse data sources, including remote sensing and detailed census data. By providing a robust analytical framework and highlighting the critical role of social factors, this study offers valuable insights that can inform more targeted and effective urban planning and public health policies. Machine learning offers more accurate and fine-scale heat vulnerability identification than traditional HVMs, enabling urban planners to understand the spatial distribution and differences in heat vulnerability more efficiently and precisely. This highlights the importance of a more integrated approach that considers both social and environmental determinants in developing effective heat mitigation strategies. Furthermore, machine learning identifies key factors related to heat vulnerability in this study. The study's findings that personal health conditions and sociodemographic characteristics play a more dominant role than environmental and infrastructural factors challenge some conventional perspectives that prioritise physical and environmental interventions (Gill et al., 2007; Liou et al., 2021; Stone et al., 2010). These allow policymakers to tailor interventions directly to the most vulnerable populations, such as by providing cooling services, enhancing medical support, and increasing public awareness by organising training modules about heat risks. Machine learning can also incorporate real-time data from remote sensing and detailed census data to formulate adaptive policies that adjust with changing data (Sohani et al., 2022), allowing for the development of dynamic intervention strategies that evolve with urban changes. With machine learning, more adaptable models can be developed for different geographic contexts through adaptive learning. Expanding geographic scope and using higher-resolution datasets can enhance the generalisability of findings, allowing for better-suited local policies. Finally, machine learning enhances the understanding of the interaction between social factors and environmental exposure through its ability to handle complex non-linear relationships, integrate multi-source data, and extract features from high-dimensional datasets, leading to urban planning decisions that simultaneously consider both the physical environment and social determinants. This integration of advanced data analytics and multidisciplinary perspectives represents a significant advancement in the field, paving the way for future research to further explore and address the multifaceted nature of heat vulnerability.

The findings of this study have substantial practical implications, particularly for policy-making and urban planning. By identifying key

factors that contribute to heat vulnerability, this research provides critical insights for developing targeted heat mitigation and adaptation strategies. Policymakers can leverage these insights to prioritise interventions aimed at improving the health and social conditions of vulnerable populations, such as the elderly and those with chronic health conditions. For example, improving heat-related health infrastructure is crucial for protecting vulnerable populations (Chen et al., 2021a). The Australian government can increase the number of air-conditioned spaces in communities, provide cooling centres for the elderly and people with chronic illnesses, and enhance the supply of emergency medical resources during extreme heat periods, thereby reducing health risks associated with high temperatures. Moreover, raising public awareness of heat risks helps prevent heat-related health issues (Wang et al., 2023). Through educational campaigns, the government can increase public understanding of heat risks and encourage people, especially those with lower levels of education, to take preventive measures during high temperatures, such as staying hydrated, avoiding outdoor activities during the hottest parts of the day, and recognising symptoms of heat-related illnesses. Enhancing access to cooling and medical resources and increasing public awareness about heat risks can significantly reduce heat-related health impacts (He et al., 2019; Lee et al., 2015). Furthermore, the study underscores the importance of integrating green infrastructure into urban planning. Cities with higher vegetation cover and green spaces exhibit lower heat vulnerability, suggesting that expanding urban green spaces can mitigate the urban heat island effect and improve the overall thermal comfort of urban environments (Gascon et al., 2016; Xiang et al., 2024).

This insight supports the development of policies that promote the creation and maintenance of green spaces, which not only provide cooling benefits but also enhance urban biodiversity and residents' well-being. This study also aligns with the Sustainable Development Goals (SDGs), particularly goals 3, 11, 13, and 15 (United Nations, 2023). This approach aids in identifying and protecting high-risk populations, thereby improving public health and well-being (Goal 3). It optimises urban planning and green space distribution, enhancing the resilience and sustainability of communities (Goal 11). Extraordinary assessment capabilities support climate action by providing scientific evidence for effective mitigation and adaptation strategies (Goal 13). Overall, this method contributes to a more sustainable and climate-resilient future.

Despite this study's efforts to enhance model accuracy, applicability, and reliability by integrating machine learning algorithms and multi-source data, several limitations may still affect the interpretation and application of its findings. Firstly, census data may not be capable of fully capturing the characteristics of population mobility and unrecorded residents. Australian census data is collected based on places of usual residence and cannot fully reflect people's movement across study units, such as commuting and working. This limitation may affect the assessment of heat vulnerability due to potential inaccuracies in capturing sociodemographic features. Additionally, there are limited numbers of undocumented populations due to factors like homelessness, language barriers, and residence in remote areas, which may result in findings that do not accurately reflect their heat vulnerability. To mitigate this limitation, future research could integrate dynamic data sources, such as mobile phone data, social media data, and municipal data, to capture dynamic information on population distribution and enrich the information about unrecorded individuals. Collaborations with non-governmental organisations could also be considered, as they can help organise survey events to collect data, enhancing the comprehensiveness of heat vulnerability assessments. Incorporating more advanced machine learning algorithms to train these dynamic multi-source datasets could also be highly beneficial. For instance, Graph Neural Networks can capture complex spatial relationships between different regions, identifying the influence of neighbourhood interactions on heat vulnerability. Moreover, Recurrent Neural Networks can be used to capture the impact of dynamic population movement patterns on heat vulnerability at different time points.

Secondly, although Landsat 8 has a high spatial resolution of 30 m, its temporal resolution is lower, with a 16-day interval. Short-term temperature variations may not be fully captured, particularly during extreme heat events. Additionally, the imaging time of Landsat 8 is during the daytime, without nighttime imaging, which may not reflect heat exposure throughout the entire day. Future studies could incorporate MODIS data and air temperature data, which have higher temporal resolutions of one day and one hour respectively, to capture rapid changes in the thermal environment. Furthermore, MODIS data also provides information on variations in both daytime and nighttime temperatures. Air temperatures complement LST because the sensations of humans to these temperatures are different, enabling a more comprehensive assessment of human exposure to extreme heat. Thirdly, although Australian capital cities exhibit a variety of geographic and climatic conditions, all of them are highly urbanised, with advanced levels of economic development, education, and infrastructure. This means that the results may not be directly applicable to less urbanised and developed regions, suggesting the need for validation of the findings across a diverse range of settings, including less developed regions or cities with lower urbanisation rates. Expanding the geographic scope could enhance the study's adaptability, applicability, and generalisability, aiding in the development of tailored and effective policies and strategies. Additionally, indicators such as land cover/use and building density can capture the broad impacts of urban development on thermal comfort characteristics, including increased heat retention and reduced ventilation. However, these indicators do not fully depict insulation and ventilation within buildings, which also play critical roles in mitigating heat vulnerability. It is essential to consider these factors in future studies to develop a more comprehensive framework for assessing thermal environments, thereby enhancing the precision and reliability of heat vulnerability results. By addressing these limitations, future research can build on this study's foundation, providing more comprehensive and universally applicable insights into heat vulnerability and informing more effective and inclusive urban planning and public health policies.

5. Conclusion

This study set out to evaluate heat vulnerability in Australian capital cities by integrating machine learning algorithms and multi-source data. The primary objective was to identify key heat vulnerability indicators and highlight regional disparities to inform urban planners and policy-makers in developing targeted mitigation and adaptation strategies.

The findings reveal that the RF algorithm is the most effective, achieving a training R^2 of 0.9179 and a testing R^2 of 0.9089, underscoring its ability to capture complex relationships within the data. Spatial analysis highlighted significant regional disparities, with higher heat vulnerability in densely populated urban areas and lower vulnerability in greener suburban and rural regions. This imbalance necessitates tailored heat mitigation strategies. Sensitivity analysis further revealed that personal health conditions and socio-demographic characteristics, such as illness status, age, and education level, play dominant roles in determining heat vulnerability, overshadowing environmental and infrastructural factors.

The findings of this study have substantial practical implications for policymakers and urban planners in mitigating heat vulnerability in Australian capital cities. Targeted healthcare interventions are essential, particularly in areas identified as highly vulnerable, where establishing cooling centres and enhancing community healthcare services can significantly reduce heat-related health risks, especially for the elderly and those with chronic conditions. Public awareness campaigns should

also be prioritised, educating vulnerable populations about the risks of heat exposure and promoting preventive measures. Expanding urban green infrastructure is another crucial step; increasing green cover, such as parks and green roofs, can help reduce urban heat island effects and improve overall urban resilience (Goonetilleke et al., 2014; Vaeztavakoli et al., 2018; Yigitcanlar, 2010). Furthermore, integrating heat mitigation strategies into urban planning, such as mandating green spaces and reflective building materials in vulnerable areas, will help in reducing heat retention and mitigating its impact. Lastly, enhancing accessibility to cooling and medical resources, particularly for the most vulnerable populations, should be part of a broader urban cooling strategy, ensuring that these groups have the support needed during extreme heat events.

The significance of this study lies in its comprehensive approach of combining machine learning with diverse data sources to provide valuable insights for urban planning and public health policies. The research confirms that improving the health and social conditions of vulnerable populations and integrating green infrastructure are crucial for mitigating heat risks. Nonetheless, the study acknowledges limitations, such as potential inaccuracies in data sources and the need for broader geographic applicability. Future research should integrate higher-resolution datasets, expand geographic scope, and employ a wider range of machine learning techniques to improve the robustness and applicability of vulnerability assessments.

In conclusion, this study advances the application of machine learning in environmental research, offering a nuanced understanding of heat vulnerability. By highlighting the critical role of social factors, it provides actionable insights for enhancing urban resilience and sustainability in the face of climate change. Future research should continue to explore the complex interplay of social and environmental determinants, further enhancing our ability to address heat vulnerability effectively.

Funding

This research received no external funding.

CRediT authorship contribution statement

Fei Li: Writing – original draft, Methodology, Investigation, Formal analysis, Data curation. **Tan Yigitcanlar:** Writing – review & editing, Supervision, Conceptualization. **Madhav Nepal:** Writing – review & editing, Supervision. **Kien Nguyen:** Writing – review & editing, Supervision. **Fatih Dur:** Writing – review & editing. **Wenda Li:** Writing – review & editing.

Declaration of competing interest

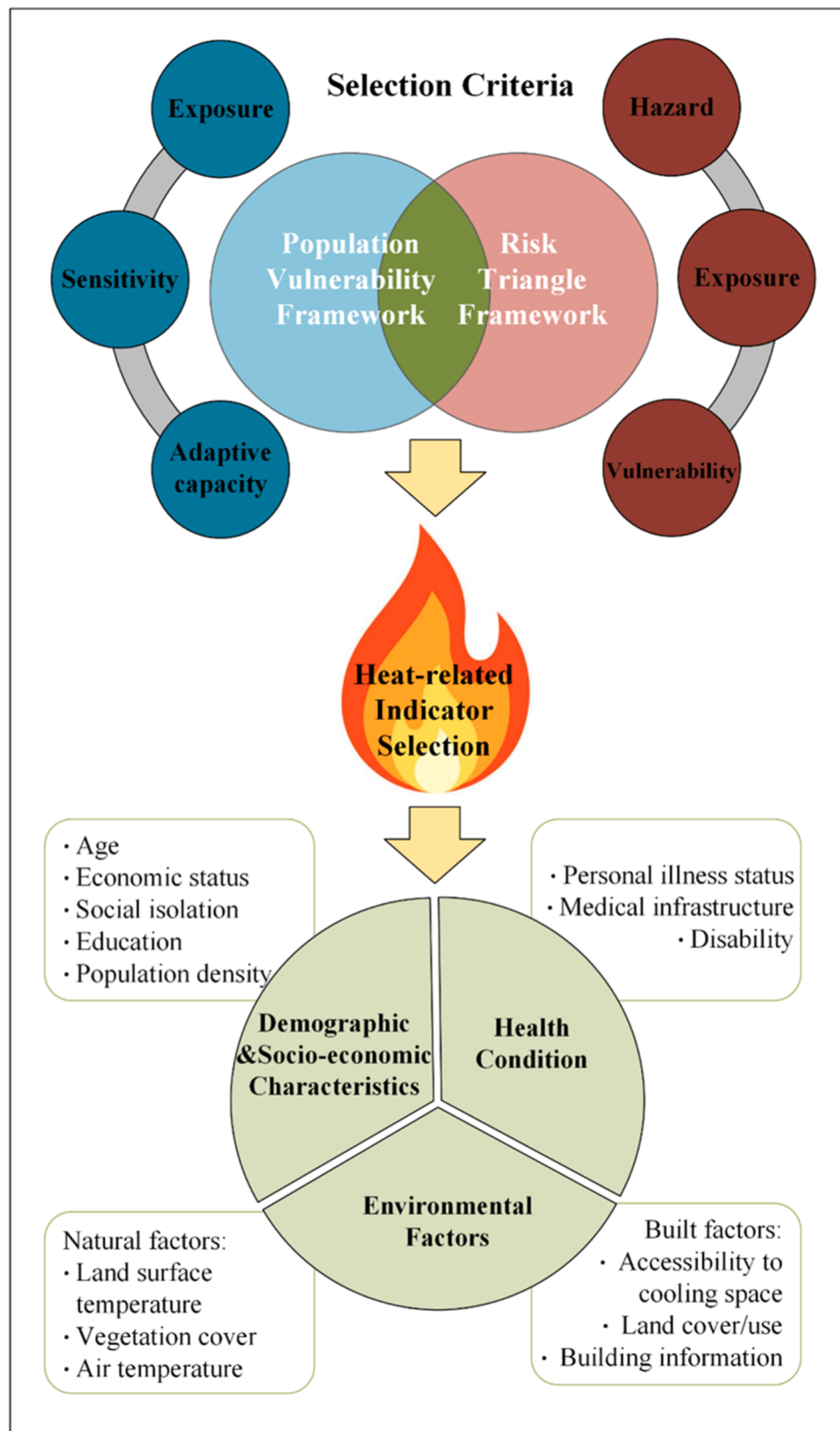
The authors declare no competing financial interests or personal relationships that could have influenced the work reported in this paper.

Acknowledgments

The authors thank Dr. Chayn Sun and her team from RMIT University, as well as Dr. Siqin Wang from the University of Southern California, for their invaluable support in data collection. We also appreciate the editor and anonymous referees for their invaluable comments on an earlier version of the manuscript. Additionally, the authors acknowledge the financial support from the Chinese Scholarship Council (No. 202106420006) and QUT towards the postgraduate research scholarship of the first named author.

Appendices

Appendix A. Heat-related Indicator Selection Conceptual Framework (Li et al., 2022, 2024a)



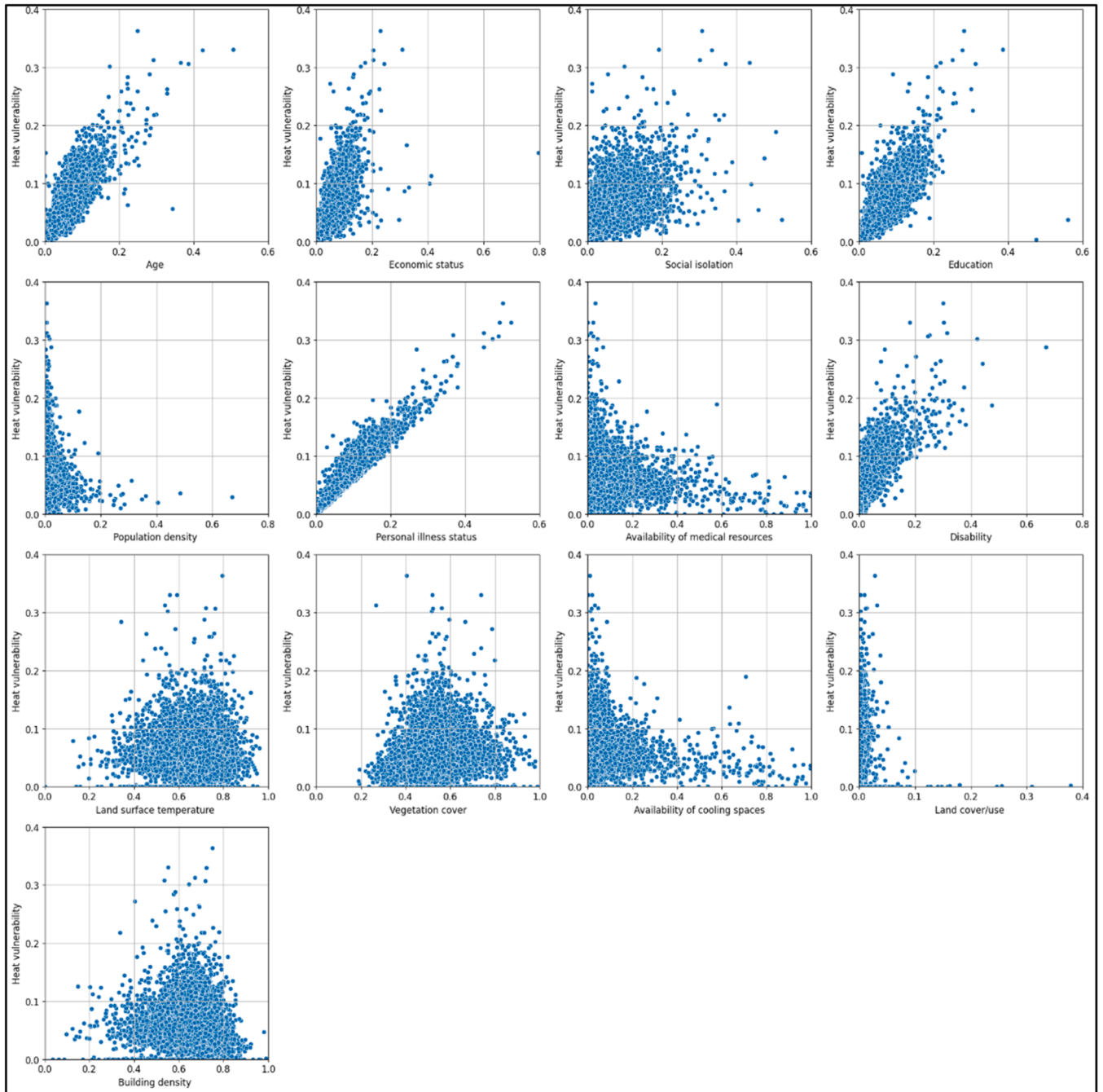
Appendix B. Heat-related death data of Australia's capital cities for validation

		NSW	VIC	QLD	SA	WA	TAS	NT	ACT
Direct Heat-Related Illnesses	Heat Stroke (X30)	2	6	6	6	6	0	6	0
	Dehydration (E86)	27	34	18	11	5	1	1	5
	Hyperpyrexia (R50.9)	0	0	2	0	0	0	0	0
Indirect Heat-Related Illnesses	Cardiovascular Diseases (R50.9)	13,659	10,198	7773	3399	3628	1200	217	548
	Respiratory Diseases (J00-J99)	4287	3103	2356	1049	1091	381	101	154
	Diabetes (E10-E14)	1735	1290	989	418	493	162	88	51
	Renal Disease (N00-N29)	973	946	421	247	240	57	38	30
	Nervous Disorders (G00-G99)	3074	2737	1815	988	1073	208	45	162
	Mental Health Conditions (F00-F99)	3661	2368	2119	995	868	278	53	165
	Total	27,418	20,682	15,499	7113	7404	2287	549	1115
Total deaths		52,485	41,093	31,367	13,607	14,993	4435	1141	2162
Death rate of total deaths (%)		52.24	50.33	49.41	52.27	49.38	51.57	48.12	51.57

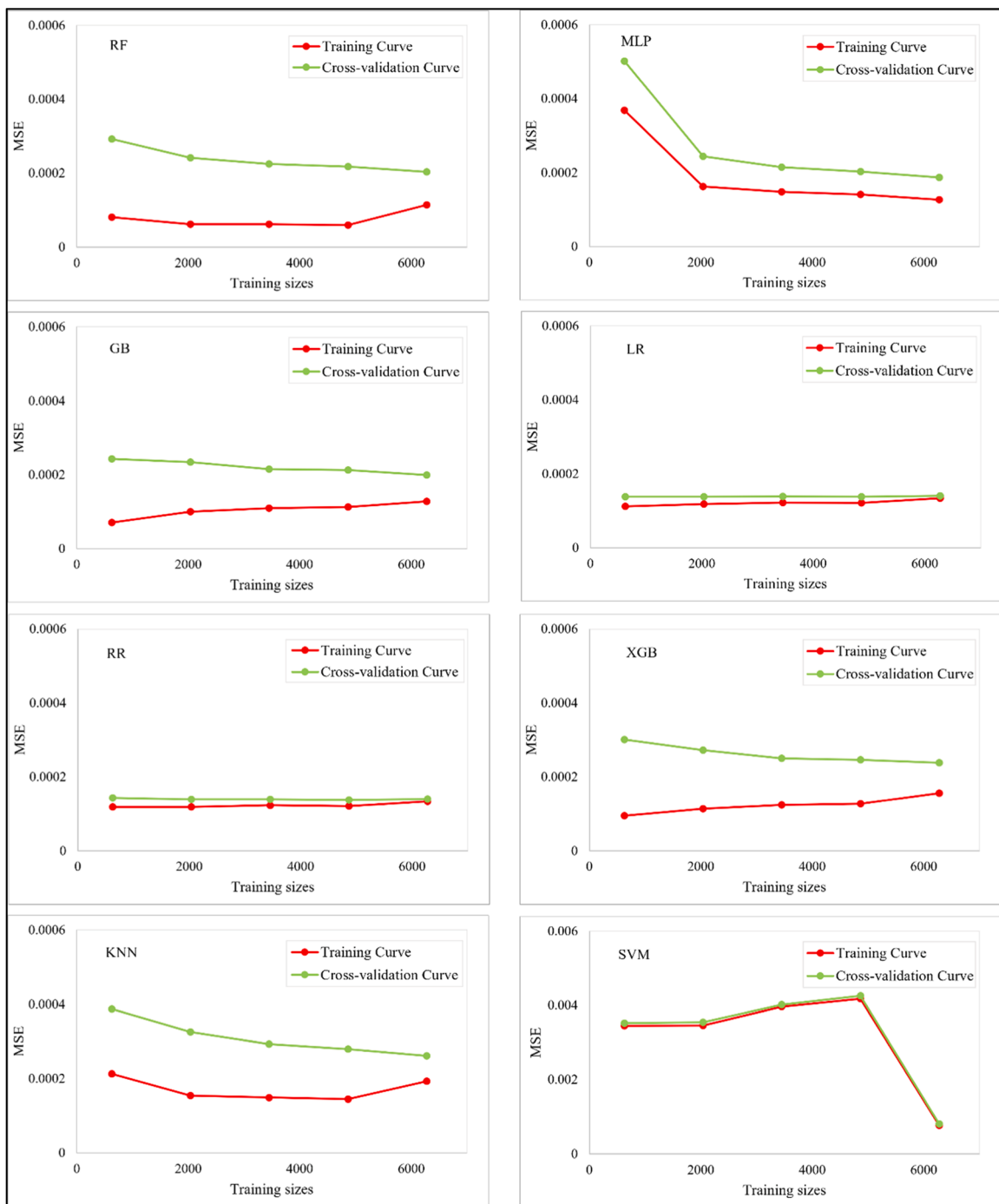
Appendix C. Collinearity diagnostics results

Indicators	Tolerance	VIF
Age	0.288	3.474
Economic status	0.394	2.535
Social isolation	0.526	1.903
Education	0.304	3.293
Population density	0.732	1.367
Personal illness status	0.162	6.177
Availability of medical resources	0.148	6.737
Disability	0.394	2.535
LST	0.569	1.756
Vegetation cover	0.284	3.525
Availability of cooling spaces	0.146	6.862
Land cover/use	0.937	1.068
Building density	0.316	3.160

Appendix D. Exploratory data analysis results - scatter plots of heat-related indicators versus labelled data



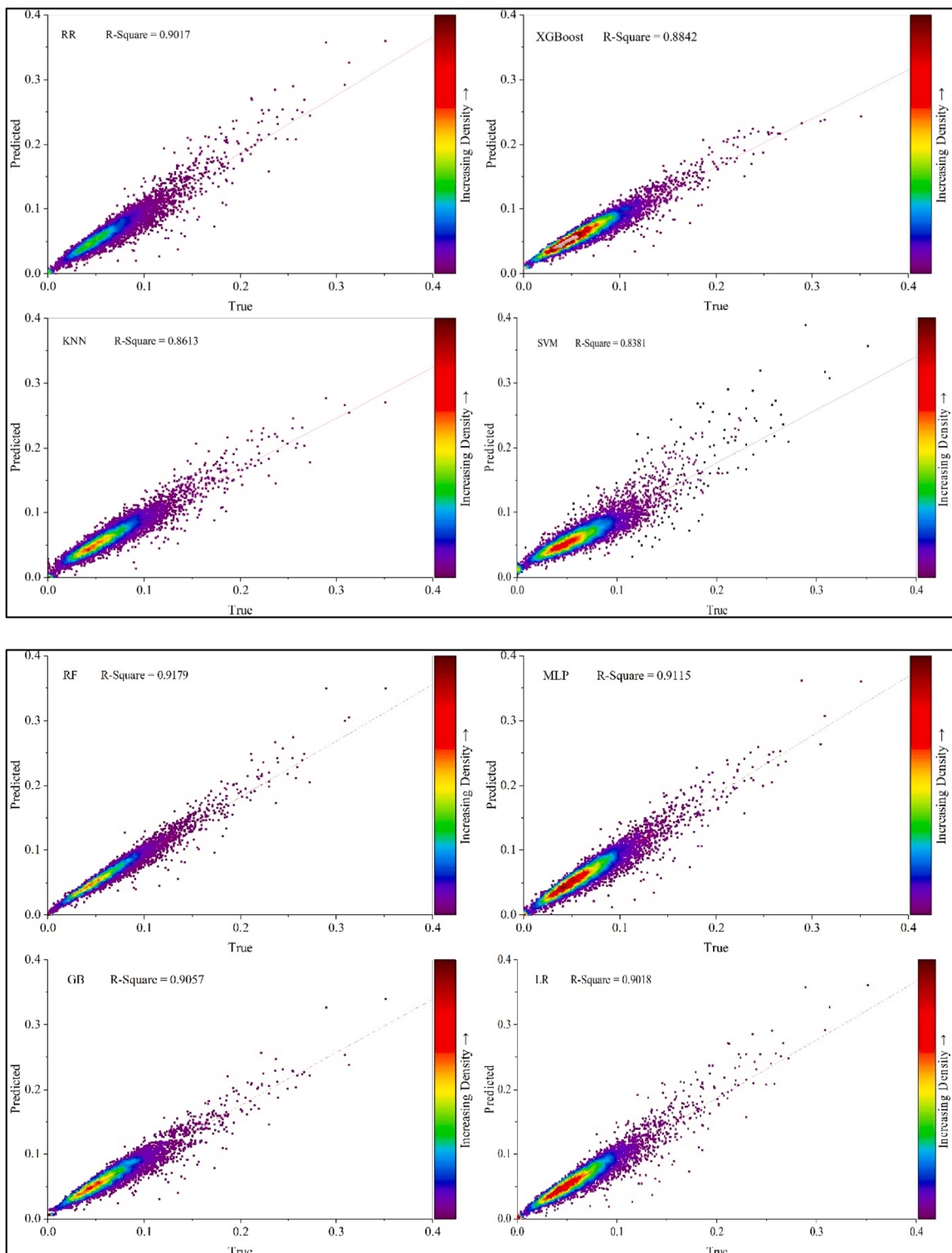
Appendix E. Learning curves of machine learning algorithms



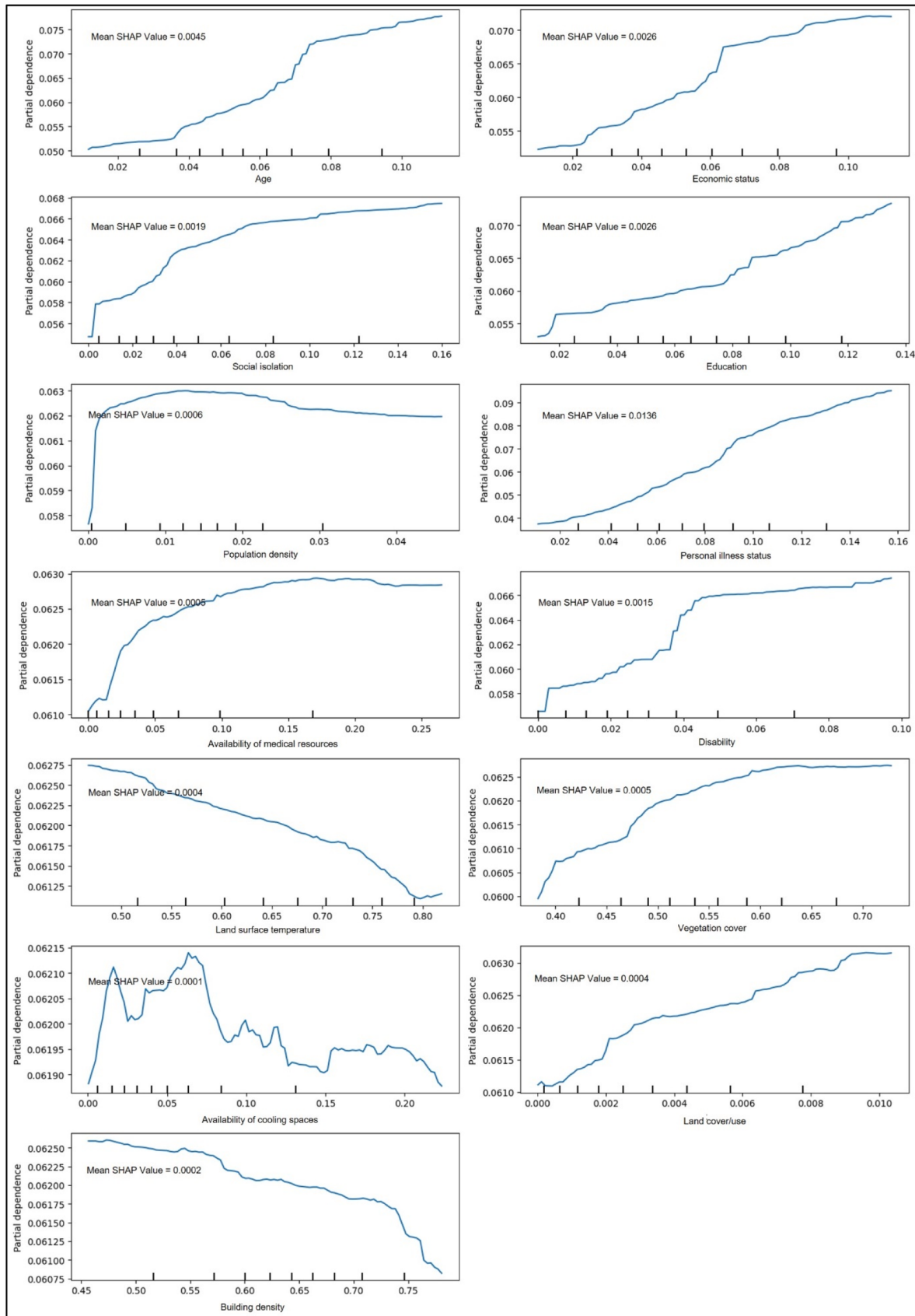
Appendix F. Hyperparameter optimisation results of machine learning algorithms

ML Algorithms	Hyperparameters	Possible Values	Optimal Values
RF	n_estimators	[100, 150, 200]	150
	max_depth	[10, 15, 20]	20
	min_samples_split	[2, 5, 10]	2
	min_samples_leaf	[1, 2, 4]	4
	max_features	['sqrt', 'log2']	log2
MLP	hidden_layer_sizes	[(50, 50, 50), (50, 100, 50), (100,)]	(50, 100, 50)
	Activation	['tanh', 'relu']	relu
	solver	['sgd', 'adam']	adam
	alpha	[0.0001, 0.05]	0.0001
	learning_rate	['constant', 'adaptive']	adaptive
GB	n_estimators	[100, 150, 200, 250, 300]	250
	learning_rate	[0.01, 0.05, 0.1]	0.01
	max_depth	[3, 4, 5]	4
	min_samples_split	[2, 5, 10]	10
	min_samples_leaf	[1, 2, 4]	2
LR	subsample	[0.8, 0.9, 1.0]	0.9
	fit_intercept	[True, False]	True
RR	alpha	[0.1, 1, 10, 100]	0.1
	fit_intercept	[True, False]	True
XGB	n_estimators	[50, 100, 150, 200, 250]	200
	learning_rate	[0.01, 0.05, 0.1]	0.01
	max_depth	[3, 4, 5]	5
	subsample	[0.8, 0.9, 1.0]	0.8
	colsample_bytree	[0.8, 0.9, 1.0]	0.8
	gamma	[0, 0.1, 0.2]	0
	reg_alpha	[0, 0.01, 0.1]	0.01
	reg_lambda	[1, 0.1, 0.01]	1
	n_neighbors	[6, 7, 8, 9, 10, 11, 12, 13, 14, 15]	7
KNN	weights	['uniform', 'distance']	Uniform
	metric	['euclidean', 'manhattan', 'minkowski']	Manhattan
	C	[0.1, 1, 10, 100, 1000]	1000
	epsilon	[0.05, 0.1, 0.15, 0.2, 0.25, 0.3, 0.4, 0.5, 0.6, 0.7]	0.1
	kernel	['linear', 'poly', 'rbf', 'sigmoid']	Poly
SVM	gamma	['scale', 'auto', 0.001, 0.01, 0.1, 1]	0.1
	degree	[2, 3, 4, 5] For 'poly' kernel	2
	coef0	[0.0, 0.5, 1, 2, 3] For 'poly' and 'sigmoid' kernels	2

Appendix G. Training results of machine learning algorithms



Appendix H. Partial Dependence Plots and Mean SHAP Values of Each Heat-related Indicator



Data availability

Data will be made available on request.

References

- Adnan, M., Dewan, A., Botje, D., Shahid, S., & Hassan, Q. K. (2022). Vulnerability of Australia to heatwaves: A systematic review on influencing factors, impacts, and mitigation options. *Environmental Research*, 213, Article 113703.
- Afzal, S., Ziapour, B. M., Shokri, A., Shakibi, H., & Sobhani, B. (2023). Building energy consumption prediction using multilayer perceptron neural network-assisted models; comparison of different optimization algorithms. *Energy*, 282, Article 128446.
- Aheto, J. M. K., Duah, H. O., Agbadi, P., & Nakua, E. K. (2021). A predictive model, and predictors of under-five child malaria prevalence in Ghana: How do LASSO, Ridge and Elastic net regression approaches compare? *Preventive Medicine Reports*, 23, Article 101475.
- Almukhalfi, H., Noor, A., & Noor, T. H. (2024). Traffic management approaches using machine learning and deep learning techniques: A survey. *Engineering Applications of Artificial Intelligence*, 133, Article 108147.
- Australian Bureau of Meteorology. (2021). National climate statement. Climate Change in Australia. Retrieved July 5, 2024, from <https://www.climatechangeaustralia.gov.au/en/changing-climate/national-climate-statement/>.
- Australian Bureau of Statistics. (2022). ABS census 2021. Retrieved June 6, 2023, from <https://www.abs.gov.au/census/find-census-data/datapacks>.
- Aubrecht, C., & Özceylan, D. (2013). Identification of heat risk patterns in the US National Capital Region by integrating heat stress and related vulnerability. *Environment International*, 56, 65–77.
- Bakhsh, K., Rauf, S., & Zulfiqar, F. (2018). Adaptation strategies for minimizing heat wave induced morbidity and its determinants. *Sustainable Cities and Society*, 41, 95–103.
- Ballester, J., Quijal-Zamorano, M., Méndez Turribiates, R. F., Pegenaute, F., Herrmann, F. R., Robine, J. M., ... Achebak, H. (2023). Heat-related mortality in Europe during the summer of 2022. *Nature Medicine*, 29(7), 1857–1866.
- Belgiu, M., & Dragut, L. (2016). Random forest in remote sensing: A review of applications and future directions. *ISPRS Journal of Photogrammetry and Remote Sensing*, 114, 24–31.
- Bu, S., Smith, K. L., Masoud, F., & Sheinbaum, A. (2024). Spatial distribution of heat vulnerability in Toronto, Canada. *Urban Climate*, 54, Article 101838.
- Cai, Z., Tang, Y., Chen, K., & Han, G. (2019). Assessing the heat vulnerability of different local climate zones in the old areas of a Chinese megacity. *Sustainability*, 11(7), 2032.
- Chambers, J. (2020). Global and cross-country analysis of exposure of vulnerable populations to heatwaves from 1980 to 2018. *Climatic Change*, 163(1), 539–558.
- Chen, Q., Ding, M., Yang, X., Hu, K., & Qi, J. (2018). Spatially explicit assessment of heat health risk by using multi-sensor remote sensing images and socioeconomic data in Yangtze River Delta, China. *International Journal of Health Geographics*, 17, 1–15.
- Chen, B., Xie, M., Feng, Q., Li, Z., Chu, L., & Liu, Q. (2021 a). Heat risk of residents in different types of communities from urban heat-exposed areas. *Science of the Total Environment*, 768, Article 145052.
- Chen, C.-C., Wang, Y.-R., Yeh, H.-Y., Lin, T.-H., Huang, C.-S., & Wu, C.-F. (2021b). Estimating monthly PM_{2.5} concentrations from satellite remote sensing data, meteorological variables, and land use data using ensemble statistical modeling and a random forest approach. *Environmental Pollution*, 291, Article 118159.
- Cheng, W., Li, D., Liu, Z., & Brown, R. D. (2021). Approaches for identifying heat-vulnerable populations and locations: A systematic review. *Science of the Total Environment*, 799, Article 149417.
- Chi, Y., Fan, M., Zhao, C., Yang, Y., Fan, H., Yang, X., ... Tao, J. (2022). Machine learning-based estimation of ground-level NO₂ concentrations over China. *Science of the Total Environment*, 807, Article 150721.
- Christenson, M., Geiger, S. D., Phillips, J., Anderson, B., Losurdo, G., & Anderson, H. A. (2017). Heat vulnerability index mapping for Milwaukee and Wisconsin. *Journal of Public Health Management and Practice*, 23(4), 396–403.
- Chuang, W. C., & Gober, P. (2015). Predicting hospitalization for heat-related illness at the census-tract level: Accuracy of a generic heat vulnerability index in phoenix, Arizona (USA). *Environmental Health Perspectives*, 123(6), 606–612.
- Coates, L., van Leeuwen, J., Browning, S., Gissing, A., Bratchell, J., & Avci, A. (2022). Heatwave fatalities in Australia, 2001–2018: An analysis of coronial records. *International Journal of Disaster Risk Reduction*, 67, Article 102671. <https://doi.org/10.1016/j.ijdr.2021.102671>
- Conlon, K. C., Mallen, E., Gronlund, C. J., Berrocal, V. J., Larsen, L., & O'Neill, M. S. (2020). Mapping human vulnerability to extreme heat: A critical assessment of heat vulnerability indices created using principal components analysis. *Environmental Health Perspectives*, 128(9), Article 097001.
- Crichton, D. (1999). The risk triangle. *Natural Disaster Management*, 102(3), 102–103.
- Degirmenci, K., Desouza, K., Fieuw, W., Watson, R., & Yigitcanlar, T. (2021). Understanding policy and technology responses in mitigating urban heat islands: A literature review and directions for future research. *Sustainable Cities and Society*, 70, Article 102873.
- Department of Human Services. (2009). *January 2009 heatwave in victoria: An assessment of health impacts*. Victorian Government Department of Human Services.
- Depietri, Y., Welle, T., & Renaud, F. G. (2013). Social vulnerability assessment of the Cologne urban area (Germany) to heat waves: Links to ecosystem services. *International Journal of Disaster Risk Reduction*, 6, 98–117.
- Economics, N.C. (2018). Heatwaves in Victoria: A vulnerability assessment. Department of Environment, Land, Water and Planning, Victoria.
- El-Zein, A., & Tommoy, F. N. (2015). Assessment of vulnerability to climate change using a multi-criteria outranking approach with application to heat stress in Sydney. *Ecological Indicators*, 48, 207–217.
- T. Elizabeth, L., Tapper, M. J., Phan, N., & McInnes, A. (2014). Can a spatial index of heat-related vulnerability predict emergency service demand in Australian capital cities? *International Journal of Emergency Services*, 3(1), 6–33.
- Estoque, R. C., Ooba, M., Seposo, X. T., Togawa, T., Hijikata, Y., Takahashi, K., & Nakamura, S. (2020). Heat health risk assessment in Philippine cities using remotely sensed data and social-ecological indicators. *Nature Communications*, 11(1), 1581.
- Fan, D., Xue, K., Zhang, R., Zhu, W., Zhang, H., Qi, J., ... Cui, P. (2024). Application of interpretable machine learning models to improve the prediction performance of ionic liquids toxicity. *Science of the Total Environment*, 908, Article 168168.
- Forceville, G., Lemonsu, A., Goria, S., Stempfelet, M., Host, S., Alessandrini, J. M., ... Pascal, M. (2024). Spatial contrasts and temporal changes in fine-scale heat exposure and vulnerability in the Paris region. *Science of the Total Environment*, 906, Article 167476.
- Gao, Y., Zhao, J., & Han, L. (2023). Quantifying the nonlinear relationship between block morphology and the surrounding thermal environment using random forest method. *Sustainable Cities and Society*, 91, Article 104443.
- Gascon, M., Triguero-Mas, M., Martínez, D., Dadvand, P., Rojas-Rueda, D., Plasencia, A., & Nieuwenhuijsen, M. J. (2016). Residential green spaces and mortality: A systematic review. *Environment International*, 86, 60–67.
- Ghaffarian, S., Roy, D., Filatova, T., & Kerle, N. (2021). Agent-based modelling of post-disaster recovery with remote sensing data. *International Journal of Disaster Risk Reduction*, 60, Article 102285.
- Gill, S. E., Handley, J. F., Ennos, A. R., & Pauleit, S. (2007). Adapting cities for climate change: The role of the green infrastructure. *Built Environment*, 33(1), 115–133.
- Green, H. K., Andrews, N., Armstrong, B., Bickler, G., & Pebody, R. (2016). Mortality during the 2013 heatwave in England—how did it compare to previous heatwaves? A retrospective observational study. *Environmental Research*, 147, 343–349.
- Goonetilleke, A., Yigitcanlar, T., Ayoko, G. A., & Egodawatta, P. (2014). *Sustainable urban water environment: Climate, pollution and adaptation* (pp. 245–346). Cheltenham, UK: Edward Elgar.
- Gudes, O., Kendall, E., Yigitcanlar, T., Pathak, V., & Baum, S. (2010). Rethinking health planning: a framework for organising information to underpin collaborative health planning. *Health Information Management Journal*, 39(2), 18–29.
- Guo, X., Huang, G., Jia, P., & Wu, J. (2019). Estimating fine-scale heat vulnerability in Beijing through two approaches: Spatial patterns, similarities, and divergence. *Remote Sensing*, 11(20), 2358.
- Harmay, N. S. M., Kim, D., & Choi, M. (2021). Urban heat island associated with land use/land cover and climate variations in Melbourne, Australia. *Sustainable Cities and Society*, 69, Article 102861.
- He, C., Ma, L., Zhou, L., Kan, H., Zhang, Y., Ma, W., & Chen, B. (2019). Exploring the mechanisms of heat wave vulnerability at the urban scale based on the application of big data and artificial societies. *Environment International*, 127, 573–583.
- Hu, K., Yang, X., Zhong, J., Fei, F., & Qi, J. (2017). Spatially explicit mapping of heat health risk utilizing environmental and socioeconomic data. *Environmental Science & Technology*, 51(3), 1498–1507.
- Hulley, G., Shivers, S., Wetherley, E., & Cudd, R. (2019). New ECOSTRESS and MODIS land surface temperature data reveal fine-scale heat vulnerability in cities: A case study for Los Angeles County, California. *Remote Sensing*, 11(18), 2136.
- Iping, A., Kidston-Lattari, J., Simpson-Young, A., Duncan, E., & McManus, P. (2019). (Re) presenting urban heat islands in Australian cities: A study of media reporting and implications for urban heat and climate change debates. *Urban Climate*, 27, 420–429.
- Lee, T. M., Markowitz, E. M., Howe, P. D., Ko, C. Y., & Leiserowitz, A. A. (2015). Predictors of public climate change awareness and risk perception around the world. *Nature Climate Change*, 5(11), 1014–1020.
- Li, F., Yigitcanlar, T., Nepal, M., Thanh, K. N., & Dur, F. (2022). Understanding urban heat vulnerability assessment methods: A PRISMA review. *Energies*, 15(19), 6998.
- Li, F., Yigitcanlar, T., Nepal, M., Nguyen, K., & Dur, F. (2023). Machine learning and remote sensing integration for leveraging urban sustainability: A review and framework. *Sustainable Cities and Society*, 96, Article 104653.
- Li, F., Yigitcanlar, T., Nepal, M., Thanh, K. N., & Dur, F. (2024a). A novel urban heat vulnerability analysis: Integrating machine learning and remote sensing for enhanced insights. *Remote Sensing*, 16(16), 3032.
- Li, F., Yigitcanlar, T., Li, W., Nepal, M., Nguyen, K., & Dur, F. (2024b). Understanding urban heat vulnerability: Scientometric analysis of five decades of research. *Urban Climate*, 56, Article 102035.
- Li, F., Yigitcanlar, T., Nepal, M., Nguyen, K., Dur, F., & Li, W. (2024c). Assessing heat vulnerability and multidimensional inequity: Lessons from indexing the performance of Australian capital cities. *Sustainable Cities and Society*, Article 105875.
- Liao, W., Fang, J., Ye, L., Bak-Jensen, B., Yang, Z., & Porte-Agel, F. (2024). Can we trust explainable artificial intelligence in wind power forecasting? *Applied Energy*, 376, Article 124273.
- Liou, Y. A., Nguyen, K. A., & Ho, L. T. (2021). Altering urban greenspace patterns and heat stress risk in Hanoi city during Master Plan 2030 implementation. *Land Use Policy*, 105, Article 105405.

- Liu, X., Yue, W., Yang, X., Hu, K., Zhang, W., & Huang, M. (2020). Mapping urban heat vulnerability of extreme heat in hangzhou via comparing two approaches. *Complexity*, 2020(1), Article 9717658.
- Liu, J., Liu, F., Zheng, C., Zhou, D., & Wang, L. (2022). Optimizing asphalt mix design through predicting the rut depth of asphalt pavement using machine learning. *Construction and Building Materials*, 356, Article 129211.
- Liu, Y., An, Z., & Ming, Y. (2024). Simulating influences of land use/land cover composition and configuration on urban heat island using machine learning. *Sustainable Cities and Society*, 108, Article 105482.
- Lu, Z., Im, J., Rhee, J., & Hodgson, M. (2014). Building type classification using spatial and landscape attributes derived from LiDAR remote sensing data. *Landscape and Urban Planning*, 130, 134–148.
- Jato-Espino, D., Manchado, C., Roldán-Valcarce, A., & Moscardó, V. (2022). ArcUHI: A GIS add-in for automated modelling of the urban heat island effect through machine learning. *Urban Climate*, 44, Article 101203.
- Kamruzzaman, M., Deilami, K., & Yigitcanlar, T. (2018). Investigating the urban heat island effect of transit oriented development in Brisbane. *Journal of Transport Geography*, 66, 116–124.
- Kan, H. J., Kharrazi, H., Chang, H. Y., Bodycombe, D., Lemke, K., & Weiner, J. P. (2019). Exploring the use of machine learning for risk adjustment: A comparison of standard and penalized linear regression models in predicting health care costs in older adults. *PloS One*, 14(3), Article e0213258.
- Karalas, K., Tsagkatakis, G., Zervakis, M., & Tsakalides, P. (2016). Land classification using remotely sensed data: Going multilabel. *IEEE Transactions on Geoscience and Remote Sensing*, 54(6), 3548–3563.
- Kim, M., Brunner, D., & Kuhlmann, G. (2021). Importance of satellite observations for high-resolution mapping of near-surface NO₂ by machine learning. *Remote Sensing of Environment*, 264, Article 112573.
- Kitchley, J. L. (2024). A framework to assess the contextual composite heat vulnerability index for a heritage city in India-A case study of Madurai. *Sustainable Cities and Society*, 101, Article 105119.
- Knowlton, K., Rotkin-Ellman, M., King, G., Margolis, H. G., Smith, D., Solomon, G., ... English, P. (2009). The 2006 California heat wave: Impacts on hospitalizations and emergency department visits. *Environmental Health Perspectives*, 117(1), 61–67.
- Kokkinos, K., Karayannis, V., Nathanail, E., & Moustakas, K. (2021). A comparative analysis of Statistical and Computational Intelligence methodologies for the prediction of traffic-induced fine particulate matter and NO₂. *Journal of Cleaner Production*, 328, Article 129500.
- Macintyre, H. L., Heavyside, C., Taylor, J., Picetti, R., Symonds, P., Cai, X. M., & Vardoulakis, S. (2018). Assessing urban population vulnerability and environmental risks across an urban area during heatwaves—Implications for health protection. *Science of the Total Environment*, 610, 678–690.
- Mallen, E., Stone, B., & Lanza, K. (2019). A methodological assessment of extreme heat mortality modeling and heat vulnerability mapping in Dallas, Texas. *Urban Climate*, 30, Article 100528.
- Marmot, M. (2005). Social determinants of health inequalities. *The Lancet*, 365(9464), 1099–1104.
- McGeehin, M. A., & Mirabelli, M. (2001). The potential impacts of climate variability and change on temperature-related morbidity and mortality in the United States. *Environmental Health Perspectives*, 109(suppl 2), 185–189.
- Meng, X., Hand, J. L., Schichtel, B. A., & Liu, Y. (2018). Space-time trends of PM_{2.5} constituents in the conterminous United States estimated by a machine learning approach, 2005–2015. *Environment International*, 121, 1137–1147.
- Modi, Y., Teli, R., Mehta, A., Shah, K., & Shah, M. (2022). A comprehensive review on intelligent traffic management using machine learning algorithms. *Innovative Infrastructure Solutions*, 7(1), 128.
- Niu, Y., Li, Z., Gao, Y., Liu, X., Xu, L., Vardoulakis, S., ... Liu, Q. (2021). A systematic review of the development and validation of the heat vulnerability index: Major factors, methods, and spatial units. *Current Climate Change Reports*, 7(3), 87–97.
- Oh, K. Y., Lee, M. J., & Jeon, S. W. (2017). Development of the Korean climate change vulnerability assessment tool (VESTAP)—Centered on health vulnerability to heat waves. *Sustainability*, 9(7), 1103.
- Okumus, D. E., & Terzi, F. (2021). Evaluating the role of urban fabric on surface urban heat island: The case of Istanbul. *Sustainable Cities and Society*, 73, Article 103128.
- Palaniyappan, B., & Vinoprala, T. (2024). Dynamic pricing for load shifting: Reducing electric vehicle charging impacts on the grid through machine learning-based demand response. *Sustainable Cities and Society*, 103, Article 105256.
- Parry, M. L. (2007). Climate change 2007-impacts, adaptation and vulnerability. In *Working group II contribution to the fourth assessment report of the IPCC* (Vol. 4). Cambridge University Press.
- Prosdocimi, D., & Klima, K. (2020). Health effects of heat vulnerability in Rio de Janeiro: A validation model for policy applications. *SN Applied Sciences*, 2, 1–11.
- Reid, C. E., O'neill, M. S., Gronlund, C. J., Brines, S. J., Brown, D. G., Diez-Roux, A. V., & Schwartz, J. (2009). Mapping community determinants of heat vulnerability. *Environmental Health Perspectives*, 117(11), 1730–1736.
- Sarimin, M., & Yigitcanlar, T. (2012). Towards a comprehensive and integrated knowledge-based urban development model: status quo and directions. *International Journal of Knowledge-Based Development*, 3(2), 175–192.
- Schlosser, A. D., Szabó, G., Bertalan, L., Varga, Z., Enyedi, P., & Szabó, S. (2020). Building extraction using orthophotos and dense point cloud derived from visual band aerial imagery based on machine learning and segmentation. *Remote Sensing*, 12(15), 2397.
- Shafizadeh-Moghadam, H., Asghari, A., Tayyebi, A., & Taleai, M. (2017). Coupling machine learning, tree-based and statistical models with cellular automata to simulate urban growth. *Computers, Environment and Urban Systems*, 64, 297–308.
- Sohani, A., Sayyaadi, H., Miremadi, S. R., Samiezafeh, S., & Doraneghard, M. H. (2022). Thermo-electro-environmental analysis of a photovoltaic solar panel using machine learning and real-time data for smart and sustainable energy generation. *Journal of Cleaner Production*, 353, Article 131611.
- Solar, O., & Irwin, A. (2010). *A conceptual framework for action on the social determinants of health*. WHO Document Production Services.
- Song, J., Huang, B., Kim, J. S., Wen, J., & Li, R. (2020). Fine-scale mapping of an evidence-based heat health risk index for high-density cities: Hong Kong as a case study. *Science of the Total Environment*, 718, Article 137226.
- Stone, B., Hess, J. J., & Frumkin, H. (2010). Urban form and extreme heat events: Are sprawling cities more vulnerable to climate change than compact cities? *Environmental Health Perspectives*, 118(10), 1425–1428.
- Tella, A., Balogun, A. L., Adebisi, N., & Abdullah, S. (2021). Spatial assessment of PM10 hotspots using random forest, K-nearest neighbour and Naïve Bayes. *Atmospheric Pollution Research*, 12(10), Article 101202.
- Tanoori, G., Soltani, A., & Modiri, A. (2024). Machine learning for urban heat island (UHI) analysis: Predicting land surface temperature (LST) in urban environments. *Urban Climate*, 55, Article 101962.
- Tate, E. (2012). Social vulnerability indices: A comparative assessment using uncertainty and sensitivity analysis. *Natural Hazards*, 63, 325–347.
- United Nations. (2023). Global indicator framework for the Sustainable Development Goals and targets of the 2030 Agenda for Sustainable Development.
- Xiao, L., Lo, S., Liu, J., Zhou, J., & Li, Q. (2021). Nonlinear and synergistic effects of tod on urban vibrancy: Applying local explanations for gradient boosting decision tree. *Sustainable Cities and Society*, 72, Article 103063.
- Yang, N., Shi, H., Tang, H., & Yang, X. (2022). Geographical and temporal encoding for improving the estimation of PM_{2.5} concentrations in China using end-to-end gradient boosting. *Remote Sensing of Environment*, 269, Article 112828.
- Vaeztavakoli, A., Lak, A., & Yigitcanlar, T. (2018). Blue and green spaces as therapeutic landscapes: Health effects of urban water canal areas of Isfahan. *Sustainability*, 10(11), 4010.
- Victorian Government Department of Environment, Land, Water and Planning. (2019). The economic impact of heatwaves on Victoria. Victorian Government. https://www.climatechange.vic.gov.au/_data/assets/pdf_file/0011/413030/The-economic-impact-of-heatwaves-on-Victoria.pdf.
- Wang, Q., Wang, X., Zhou, Y., Liu, D., & Wang, H. (2022a). The dominant factors and influence of urban characteristics on land surface temperature using random forest algorithm. *Sustainable Cities and Society*, 79, Article 103722.
- Wang, E., Xia, J., Li, J., Sun, X., & Li, H. (2022b). Parameters exploration of SOFC for dynamic simulation using adaptive chaotic grey wolf optimization algorithm. *Energy*, 261, Article 125146.
- Wang, S., Sun, Q. C., Huang, X., Tao, Y., Dong, C., Das, S., & Liu, Y. (2023). Health-integrated heat risk assessment in Australian cities. *Environmental Impact Assessment Review*, 102, Article 107176.
- Weber, S., Sadoff, N., Zell, E., & de Sherbinin, A. (2015). Policy-relevant indicators for mapping the vulnerability of urban populations to extreme heat events: A case study of Philadelphia. *Applied Geography*, 63, 231–243.
- Wu, X., Liu, Q., Huang, C., & Li, H. (2022). Mapping heat-health vulnerability based on remote sensing: A case study in Karachi. *Remote Sensing*, 14(7), 1590.
- Xiang, Y., Yuan, C., Cen, Q., Huang, C., Wu, C., Teng, M., & Zhou, Z. (2024). Heat risk assessment and response to green infrastructure based on local climate zones. *Building and Environment*, 248, Article 111040.
- Ye, T., Zhao, N., Yang, X., Ouyang, Z., Liu, X., Chen, Q., ... Jia, P. (2019). Improved population mapping for China using remotely sensed and points-of-interest data within a random forests model. *The Science of the Total Environment*, 658, 936–946.
- Yigitcanlar, T. (2010). *Rethinking sustainable development: Urban management, engineering, and design*. Hersey, PA: IGI Global.
- Yigitcanlar, T., Degirmenci, K., Butler, L., & Desouza, K. (2022). What are the key factors affecting smart city transformation readiness? Evidence from Australian cities. *Cities*, 120, 103434.
- Yu, Q., Yue, D., Wang, J., Zhang, Q., Li, Y., Yu, Y., ... Li, N. (2017). The optimization of urban ecological infrastructure network based on the changes of county landscape patterns: A typical case study of ecological fragile zone located at Deng Kou (Inner Mongolia). *Journal of Cleaner Production*, 163, S54–S67.
- Zhang, C., Pan, X., Li, H., Gardiner, A., Sargent, I., Hare, J., & Atkinson, P. M. (2018). A hybrid MLP-CNN classifier for very fine resolution remotely sensed image classification. *ISPRS Journal of Photogrammetry and Remote Sensing*, 140, 133–144.
- Zhao, J., Ji, G., Tian, Y., Chen, Y., & Wang, Z. (2018). Environmental vulnerability assessment for mainland China based on entropy method. *Ecological Indicators*, 91, 410–422.
- Zhao, P., Zhu, N., Chong, D., & Hou, Y. (2022). Developing a new heat strain evaluation index to classify and predict human thermal risk in hot and humid environments. *Sustainable Cities and Society*, 76, Article 103440.
- Zhou, Z., Yu, L., Wang, Y., Tian, Y., & Li, X. (2024). Innovative approach to daily carbon dioxide emission forecast based on ensemble of quantile regression and attention BILSTM. *Journal of Cleaner Production*, 460, Article 142605.